Modelling of Phototrophic Purple Bacteria Growth across Different Metabolic Modes

Kornél Kiss

TU Delft

Modelling of Phototrophic Purple Bacteria Growth across Different Metabolic Modes

By

Kornél Kiss

Student Number - 6103448

Faculty of Civil Engineering and Geosciences

MSc Environmental Engineering - Water Resources Engineering Track

Delft University of Technology

The Netherlands

Defended publicly on November 6, 2025 at 10:00

Graduation Committee:

Chair - Ralph Lindeboom

Second Assessor - Samarpita Roy

Third Assessor - Michele Laureni

Preface

This thesis marks the end of my Master's studies in Environmental Engineering at Delft University of Technology. My time in Delft feels simultaneously both shorter and longer than just two years. It was sometimes hard, but I gained a little knowledge about a wide range of interesting topics, many of which I did not even know existed before. My master's thesis was similarly challenging, often an exercise in not knowing what I did not know, but I learned a lot. It would not have been possible without the support, guidance, and encouragement of many people.

First and foremost, I would like to thank my supervisor, Ralph Lindeboom, for his guidance and for patiently answering my countless questions during our weekly meetings. I am especially grateful for all the freedom he gave me to explore and define my own thesis topic, as well as for his advice on how to refine my ideas into feasible research.

I am grateful to Manuel Godoy for providing access to the data from his earlier research, which served as a valuable foundation for this thesis.

I would like to thank my co-supervisors, Samarpita Roy and Michele Laureni, for their constructive feedback during the milestone presentations of my thesis. I am also grateful to Armand Middledorp for helping me get oriented in the lab, demonstrating the use of various instruments, and patiently answering countless "just one more questions". My thanks go as well to Jing Zha, who generously spent afternoons teaching me how to conduct experiments and meticulously pointing out pitfalls and tricks to make them as consistent and straightforward as possible. I would also like to thank Helena Moreira and Fauzul Imron for their help in the lab, for answering my many questions about the whereabouts of things, and for making the time pass more quickly while working in the lab.

Finally, I would like to thank my family and friends for their support and encouragement throughout my studies.

Kornél Kiss
Delft, October 2025

Summary

Rhodospirillum rubrum is a phototrophic purple bacterium with a high degree of metabolic flexibility, capable of growing under a wide range of environmental conditions. It also has many potential industrial applications, such as hydrogen and bioplastic production. However, the main obstacles preventing large-scale implementation of these applications are the limited practical knowledge of the bacterium's growth under changing environmental conditions, and the high electricity demand required for during photosynthesis, which makes its cultivation costly.

In this thesis, a simple, general, and expandable mathematical model is developed that builds on currently available data from the literature and aims to describe *R. rubrum* growth under both anaerobic dark and light conditions. It accounts for multiple metabolic states based on the available substrates and the supplementation with carbon monoxide.

The first part of the thesis reviews existing literature. Different mathematical frameworks used to describe microbial growth are examined, with a focus on unstructured models that assume constant bacterial properties. These models are compared and evaluated based on their suitability. A clear distinction is made between the lag phase, when growth is essentially zero due to the bacteria adjusting to the changed environmental conditions, and substrate inhibition at high concentrations, when growth is slowed until the concentration falls below a threshold. The most significant parameters influencing growth are identified.

Next, the experimental setup is presented. This includes a description of a batch reactor configuration (stirring, lighting, heating, and medium) as well as the measurement methods. This is followed by a detailed description of the mathematical growth model as implemented. The model parameters, such as half-saturation constants, substrate inhibition values, and variables related to lag-phase length are extrapolated from extracted data of published research.

This is followed by the comparison of training data and model prediction, the presentation of the collected experimental data, and the model is compared to the experimental data. The experiments demonstrate the utility of the conceptual model under anaerobic light conditions, however, its accuracy is limited by the quality of the data used to estimate model parameters, particularly yields. For anaerobic dark conditions, the experimental results differ significantly from expectations based on literature. In particular, bacterial growth appeared to rely only on carbon (and likely starch extract), rather than on carbon monoxide and acetate. The exact reason for this discrepancy remains unclear, however it can be assumed with reasonable confidence that it is due to the experimental setup and measuring frequency and length and not an error in the model. A short comparison of potential optimization strategies is included, based on the effect of different reactor setups, assuming that the differences between expected and observed behavior could be resolved.

Finally, the relevance of the proposed model within the context of existing literature is discussed. Although the quantitative results of the model are not yet directly applicable, the proposed modeling framework, together with the estimated growth parameters, mathematical treatment of lag phases and metabolic state transitions, and comparative analysis of the optimality of different reactor setups, could provide a foundation for future refinement. In addition, it could possibly offer a unifying structure that can facilitate the integration of other, existing models operating at different scales and focuses.

Nomenclature

Abbreviations

Abbreviation	Definition
R. rubrum	*Rhodospirillum rubrum*
D1	Dark 1 (metabolic state): anaerobic respiration, in dark, using acetate and CO, producing CO_2 and H_2
L1	Light 1 (metabolic state): anaerobic photosynthesis, under light, using acetate, producing CO_2
L2	Light 2 (metabolic state): anaerobic photosynthesis, under light, using acetate and CO, producing CO_2
L3	Light 3 (metabolic state): anaerobic photosynthesis, under light, using CO_2 and H_2
OD660	Absorbance at 660 nm
PHB	Polyhydroxybutyrate
PPB	Purple photosynthetic bacteria
VFA	Volatile fatty acids
VSS	Volatile suspended solids

Symbols

Symbol	Definition	Unit
μ	Specific growth rate	day^{-1}
μ_{max}	Maximum specific growth rate	day^{-1}
K_s	Half-saturation constant	$mmol \cdot L^{-1}$
K_i	Inhibition constant	$mmol \cdot L^{-1}$
m	Fixed fraction of energy used for cell maintenance	$-$
$\mu_x^{\max}$	Specific growth rate of metabolic state x	day^{-1}
$K_{s,y}^x$	Half-saturation coefficient of substrate y in metabolic state y	$mmol \cdot L^{-1}$
$K_{i,j}^i$	Inhibition coefficient of substrate y in metabolic state x	$mmol \cdot L^{-1}$
Y_y^x	Yield of compound y per unit biomass in metabolic state x	$mmol \cdot C - mmol^{-1}$
τ_x	Constant lag phase length of metabolic state x	day

Symbol	Definition	Unit
k_x	Vertical scaler parameter of CO concentration dependent lag phase length in metabolic state x	$-$
β_x	Horizontal scaler parameter of CO concentration dependent lag phase length in metabolic state x	$-$
θ_y	Threshold concentration above which compound y considered present in the system	$mmol \cdot L^{-1}$
θ_{CO}^{cut}	Cutoff CO concentration value above which metabolic state L3 is not possible	$mmol \cdot L^{-1}$
$d_{default}$	Decay rate	day^{-1}
t	Time from the start of the reactor	day
$t_{0,i}$	Time of the start of metabolic state of i	day
Irr	Average irradiation within the reactor	$W \cdot m^{-2}$
X	Biomass concentration	$C - mmol \cdot L^{-1}$
C_i	Concentration of substrate i	$mmol \cdot L^{-1}$
$C_{CO_2}^{gas}$	Concentration of gas i in the headspace	$mmol \cdot L^{-1}$
V	Total reactor volume	L
V_{liq}	Liquid volume	L
V_{gas}	Headspace volume	L
$k_{L,y}a$	Volumetric mass-transfer rate of compound y	$-$
H_y^{cc}	Dimensionless Henry's law constants	$-$
x	Distance within the reactor from its wall	m
r	Reactor radius	m
λ	Wavelength	nm
Irr_0	Measured irradiation at the wall of the reactor	$W \cdot m^{-2}$
A	Absorbance	$-$
T	Reactor temperature	K
R	Gas constant	$8.314\mathrm{J/mol{\cdot}K}$
$H_s(T)$	Henry's constant at temperature T	$-$
H_s°	Henry's constant at reference temperature $T^\circ = 298.15K$	$-$
$\Delta_{\text{sol}}H$	Enthalpy of dissolution	$J \cdot mol^{-1}$

Contents

1. Introduction

Phototrophic Purple Bacteria (PPB) are a metabolically flexible group of microorganisms capable of adapting to a wide range of aquatic environmental conditions. They can thrive under varying light intensities, oxygen levels, and nutrient availabilities. The cultivation of one specific member of this group, *Rhodospirillum rubrum*, is of particular interest due to its many potential industrial applications.

1.1. Metabolic Modes of *R. rubrum*

Depending on environmental conditions, *R. rubrum* can switch between several distinct metabolic modes. Under aerobic respiration, which occurs in the presence of oxygen and irrespective of illumination, the organism grows chemoorganoheterotrophically by oxidizing organic substrates. In this state, the cells appear mostly colorless because the synthesis of photosynthetic pigments is repressed [1], [2].

When light is available and all oxygen has been reduced, *R. rubrum* shifts to anaerobic photosynthesis. The cells display varying pigmentation depending on the light spectrum and intensity, in order to maximize light absorption for energy production. Growth may occur in several forms: photoorganoheterotrophic, where both the electron donor and carbon source are organic molecules such as acetate or succinate, photolithoautotrophic, where both are inorganic, for example hydrogen as the electron donor and carbon dioxide as the carbon source, or photolithoheterotrophic, where the electron donor is inorganic, such as carbon monoxide, and the carbon source is organic, such as acetate [3], [4].

Under anaerobic respiration, which takes place in the absence of both oxygen and light but in the presence of alternative electron acceptors, *R. rubrum* can continue to grow. It cannot grow chemoorganoheterotrophically, but under certain conditions it can use carbon monoxide as an electron donor and organic molecules such as acetate as a carbon source to grow chemolithoheterotrophically [4], [5], [6].

Finally, during fermentation, *R. rubrum* is able to metabolize certain sugars, such as fructose or pyruvate, although growth under these conditions is considerably slower than in the other metabolic modes [5].

Table 1 shows the different metabolic modes and their trophic types.

Table 1: Summary of main metabolic modes of *R. rubrum*

Metabolic Mode	Light	Energy Source	e^- Donor	Carbon Source	Oxygen Present	Trophic Type
Aerobic respiration	Both	Chemical	Organic	Organic	Yes	Chemoorganoheterotrophic

Metabolic Mode	Light	Energy Source	e^- Donor	Carbon Source	Oxygen Present	Trophic Type
Anaerobic photosynthesis	Yes	Light	Organic or inorganic	Organic or inorganic	No	Photoorganoheterotrophic or Photolithoautotrophic or Photolitho-heterotrophic
Anaerobic respiration	No	Chemical	Organic or inorganic	Organic or inorganic	No	Chemolithoheterotrophic
Fermentation	No	Chemical	Organic	Organic	No	Chemoorganoheterotrophic

1.2. Potential Industrial Use of *R. rubrum*

The broad range of potential industrial applications is enabled by this versatility, even compared to other PPB species. These include, but not limited to:

Table 2: The different existing and potential industrial applications of *R. rubrum*

Use Case	Description
Wastewater treatment	*R. rubrum* shows potential to enhance biomass recycling and improve to the purification of wastewater treatment systems [7].
Hydrogen production	*R. rubrum* can be cultivated on syngas, a mixture of CO, H_2, and CO_2, produced through the gasification of organic waste. *R. rubrum* is capable to convert the CO of the syngas into more H_2, and CO_2 gases throught the water-gas shift reaction. With some refinement, this could potentially become a renewable energy source [4].
Bioplastic synthesis	*R. rubrum* can produce polyhydroxyalkanoates (PHAs), a type of biodegradable polymer to store energy for later use. These bioplastics can be used in place of petroleum-derived plastics, providing a more sustainable alternative[8].
Production of coenzyme Q10	*R. rubrum* is capable of synthesizing coenzyme Q10, a compound used in the pharmaceutical and cosmetic industries for its antioxidant properties [9].
Production of natural dyes for textiles	Pigments produced by *R. rubrum* can be extracted and utilized as natural dyes for textiles, offering an eco-friendly alternative to many synthetic dyes that are often harmful [10] [11].

1.3. Problem Statement

The ability to harness the potential of *R. rubrum*, and to make the listed applications economically feasible, heavily relies on a deeper understanding of its metabolism and the ability to reliably predict its behavior under changing environmental conditions within an engineering framework.

For example, the fastest growth can be achieved under photosynthesis, unfortunately, this requires continuous illumination, which is energy-intensive. An alternative could be anaerobic respiration, which does not require light but needs external supplementation of electron donors such as carbon monoxide and overall more substrates for the same growth. In order to compare which one is better for a certain set of given condition, accurate models would be needed.

One potential, more sophisticated way to minimize energy consumption and make *R. rubrum* cultivation more cost-effective is the strategic cycling of different metabolic modes. The main limitation, however, is that very few studies have investigated the transitions between metabolic modes and how the organism behaves during these shifts, for example, the length of lag phases or the precise relationship between absorbance measurements and biomass concentration under dynamic environmental conditions. To implement this within industrial setting would require an accurate model that is capable of modelling more than one metabolic modes together with the transitional periods between them.

1.4. Research Questions

The problem statement raises many potential research questions, some of them which I attempt to (partially) address within this work:

- How can the metabolic behavior of *R. rubrum* be described mathematically, for now within a small subset of its possible metabolic modes, including the transitions between them, under anaerobic conditions with varying light intensity, when carbon monoxide and acetate are the only possibly available substrates at the start of the reactor run?
- Can cultivation efficiency be improved through strategic cycling of metabolic modes, and how does this compare to continuous anaerobic photosynthesis?
- What are the computational and practical limitations of the developed system?

2. Background Literature

To answer the stated research questions, information must be collected on the different types of existing mathematical models used to describe microbial growth, and the most important variables in relation to the growth of *R. rubrum*.

2.1. Different Mathematical Models for Microbial Growth

The microbial growth process usually has four phases[12], as illustrated in Figure 1. First, in the lag phase, bacteria acclimatize to the new environment, adjusting to factors such as salinity, pH, temperature, and available substrate, for which they must begin enzyme production. During this phase, there is little to no growth. No growth might be also happen in the beginning of the growth phase due to the inhibitory effects of the initial high substrate concentrations, which must be gradually consumed before faster growth can occur. In the exponential phase, most growth occurs without significant limitations from substrate availability or inhibition due to excessively high concentrations. Next, in the stationary phase, growth slows down due to substrate or nutrient limitations, or from the accumulation of toxic byproducts. At some point, the energy required for maintenance exceeds the energy bacteria can produce, leading to cell death eventually outpacing growth. Finally, in the decay phase, the substrate has been depleted, preventing further growth, and biomass steadily decreases [12], [13].

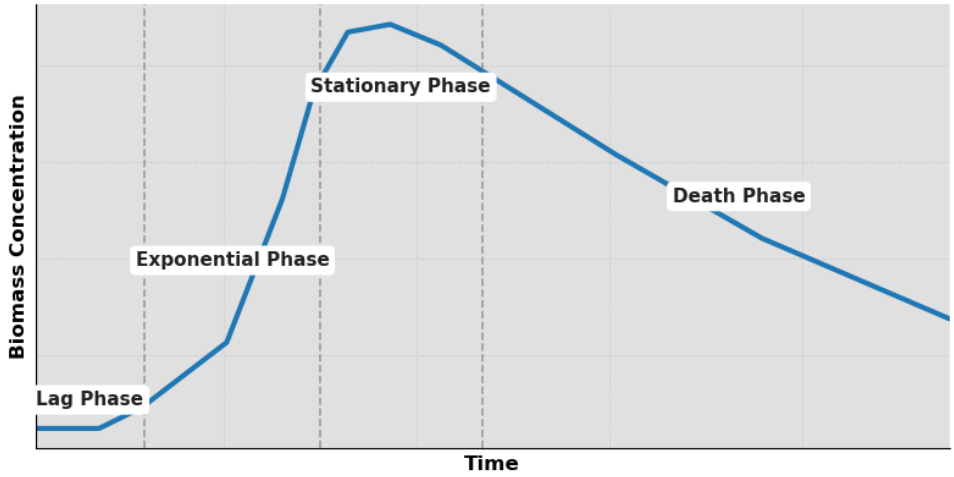

Figure 1: Microbial growth phases

There are two types of growth models used to simulate microbial kinetics: structured and unstructured models. Structured models consider genetic, morphological and biochemical properties of the biomass. Unstructured models consider bacteria as something with constant attributes, with its behavior as a function of its own and the available substrate concentrations [14]. Given the scope and engineering focus of this thesis, it was decided early on that the unstructured modelling approach would be taken [1].

[1] In general, unstructured models can only describe the behavior of so-called balanced growth. Balanced growth refers to

There are many different unstructured model used to simulate microbial growth. A short summary of some of the most common ones are presented in Table 3.

Table 3: Comparison of some of the most common and distinct unstructured microbial growth models

Model	Growth Rate of Biomass [μ]	Properties
Monod	$\mu = \mu_{max} \cdot \frac{S}{S + K_s}$ (1)	One of the first microbial growth models invented. At low substrate concentrations, it follows first-order kinetics, while at high substrate concentrations, it follows zero-order kinetics. It does not simulate the lag or decay phases and usually overestimates growth. It is suitable for simulating growth under high substrate concentrations without adverse conditions causing inhibition[13].
Monod-Ierusalimsky	$\mu = \mu_{max} \cdot \frac{S}{S + K_s} \cdot \frac{K_i}{S + K_i}$ (2)	An extension of the Monod model, it assumes some inhibition by the substrate at all substrate concentrations, with stronger inhibition at higher concentrations [15].

growth that produces cells of identical quality [15]. This is not strictly true when modeling *R. rubrum*'s behavior across different metabolic modes. For example, the length of the lag phase when transitioning between metabolic modes changes due to evolutionary adaptations based on the history of the biomass sample. To enable unstructured modeling, the following restriction was applied: every reactor run is inoculated from the same large batch of refrigerated biomass. To generalize this simplified model and make it more applicable to industrial use, the adaptability range of *R. rubrum* should be further investigated and incorporated into the model as an additional dimension

Model	Growth Rate of Biomass [μ]		Properties
Haldane	$$\mu = \mu_{max} \cdot \frac{S}{S + K_s + \frac{S^2}{K_i}}$$	(3)	Another extension of the Monod kinetics. It focuses the inhibition phase at high substrate concentration [13] . It has been show for many different microbial kinetics provide good fits to collected experimental data from phenol degradation to nitrification inhibition by ammonium [14]. The Haldane model has many variations (e.g. Webb, Yano-Koga) not presented here, that mainly differ in by raising the power of on the substrate concentration over the substrate inhibition constant. This result in stronger modeled inhibitons.
Aiba	$$\mu = \mu_{max} \cdot \frac{S}{S + K_s} \cdot e^{-S/K_i}$$	(4)	Yet another extension of the Monod model designed to address inhibition, this time using an exponential ratio of the substrate concentration to the inhibitory constant. This model has provided good fits for many biodegradation and polymer production experiments [14].
Teissier	$$\mu = \mu_{max} \cdot \left(1 - e^{-S/K_s}\right)$$	(5)	It assumes that the specific growth rate is inversely proportional to its value relative to the maximum growth rate. Tessier's model behaves similarly to Monod's at both low and high substrate concentrations and assumes no inhibition at high concentrations. The main difference lies in the transitional period from first-order to zero-order kinetics [13].

Model	Growth Rate of Biomass [μ]	Properties
Powell	$$\mu = \frac{(\mu_{max} + m)\, S}{S + K_s} - m \quad (6)$$	This is also a modification of the Monod model. It does not address inhibition but introduces a parameter m to simulate the energy requirement for maintenance. This model has not proven to be a particularly good fit for simulating any specific biological process [14].

2.2. Metabolic States

As presented in the introduction, *R. rubrum* is capable of a wide range of metabolic modes. From an industrial perspective, the most interesting of these are anaerobic photosynthesis and anaerobic respiration due to their relatively high growth rates compared to other metabolic modes and their potential for hydrogen production, one of the main possible industrial applications.

Within these two modes, in this section, different metetabolic states are defined, indicating different substrate utilization, three in anaerobic photosynthesis, and one in anaerobic respiration. Due to the limited scope of this thesis, the model was created assuming that only a limited number of potential substrates are available for growth, namely acetate, carbon monoxide, hydrogen, and carbon dioxide, as the relationships among these substrates have received some attention in the past [4], [8], [16], [17].

Among these studies, one of the most recent by Godoy et al. [4] incorporates many of the latest findings. In this study, *R. rubrum* was grown on acetate and supplemented with varying levels of CO (ranging from 0 to 2.5 bar partial pressure) under both light and dark conditions. The most relevant aspect of this study for this thesis is that it recorded the entire growth cycle, from the very beginning of the lag phase to, in most cases, the death phase when biomass concentrations began to decrease. In addition to biomass measurements, changes in the concentrations of all relevant substrates (acetate, CO, CO_2, and H_2) were also recorded under these conditions.

In the study three different states under anaerobic photosynthesis have been observed and one in the dark under anaerobic respiration as summarized in Table 4.

Table 4: Classification of the metabolic states observed in the study by Godoy et al. [4]

State	Trophic Type	Light	Energy Source	e^- Donor	Carbon Source	Products
L1	Photoorganoheterotrophy	Yes	Light	Acetate	Acetate	CO_2
L2	Photolithoheterotrophy	Yes	Light	CO	Acetate	CO_2, H_2
L3	Photolithoautotrophy	Yes	Light	H_2	CO_2	

State	Trophic Type	Light	Energy Source	e⁻ Donor	Carbon Source	Products
D1	Chemolithoheterotrophy	No	Chemical	CO	Acetate	CO_2, H_2

Under dark conditions, the one metabolic state, D1, was observed, with CO being consumed at a much higher rate than acetate [4], in comparison L2 metabolic state with the exact same substrates, under light conditions, but with photoheterotropy instead of chemoheterotropy. No growth occurs in the dark without CO supplementation [4], [6], unlike the L1 state under light conditions.

Under light, after the L2 state, when the CO concentration dropped below a certain threshold, θ_{CO}^{cut} , a second growth state, L3, was observed, utilizing the CO_2 and H_2 produced during the L2 state from CO and water.

CO concentrations also had a significant effect on the duration of the lag phases preceding the L2 and D1 states, as well as on their maximum growth rates.

The time series from the different reactor runs are shown in Figure 2.

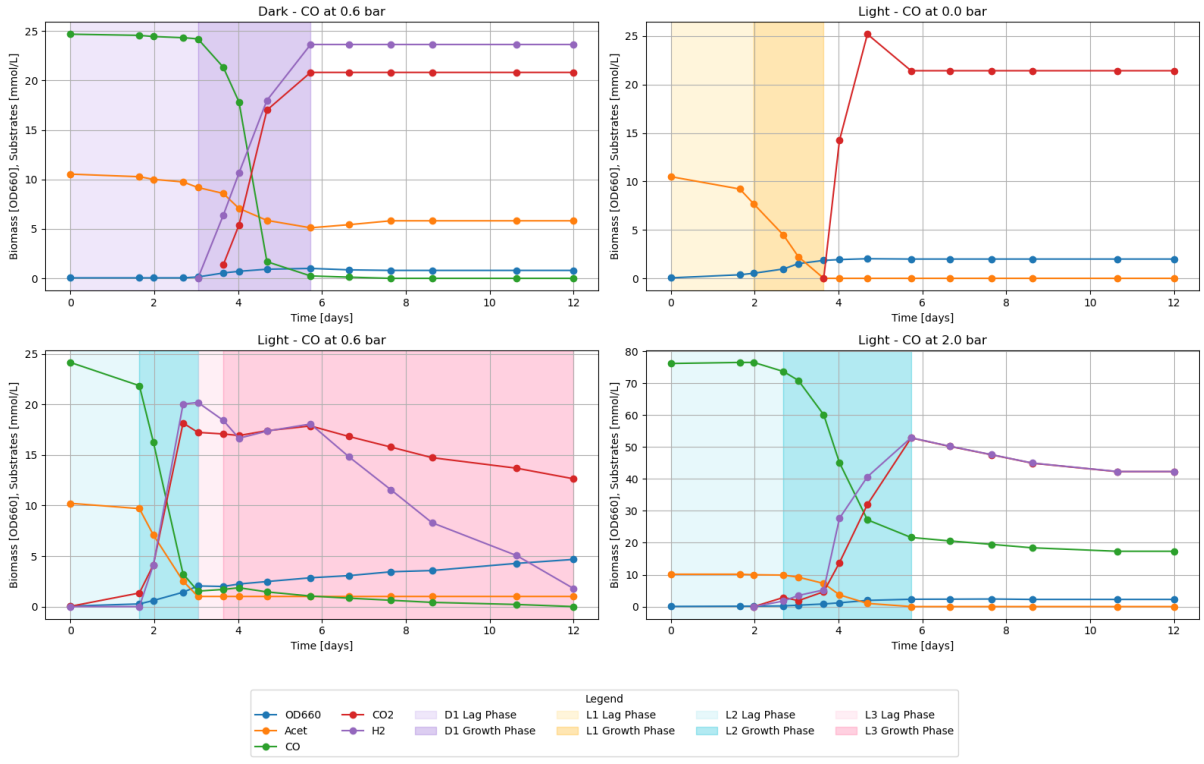

Figure 2: Classification overlayed on top of the collected data of the study by Godoy et al. [4]

2.3. Substrates and Light

Many different factors could be considered as input variables for the model. Given the scope and time limitations of this work, the focus was restricted to the substrates used during metabolic states L1, L2,

L3, and D1, as well as illumination[2]. Some other factors that could, and likely should be considered before any industrial implementation of the model are listed in Section A.1.

2.3.1. Acetate

Acetate is one of the most commonly used substrates for the cultivation of *R. rubrum* in the available literature. Bayon-Vincente et al. [18] showed that after long-term cultivation with certain VFAs including acetate, *R. rubrum* acclimates to it as a carbon source, which results in significantly reduced lag phases. A study by Ruknonsaeng et al. [19], which investigated the effects of nitrogen, acetate, and propionate on hydrogen production, reported that high concentrations of volatile fatty acids, including acetate, can lead to a decrease in pH, which subsequently inhibits *R. rubrum* growth.

Ghasem et al. [17] examined the effect of different initial acetate concentrations on the growth of *R. rubrum* under illumination, using a constant initial carbon monoxide partial pressure of 0.6 bar. This would be L2 state, according to the classification in Table 4. Their results showed that acetate exhibits both a growth-limiting concentration threshold, somewhere bellow 8 mmol · L^{-1}, below which the growth rate is significantly reduced, and an inhibitory effect at higher concentrations, above 35 mmol · L^{-1}, likely due to substrate toxicity and not just pH change.

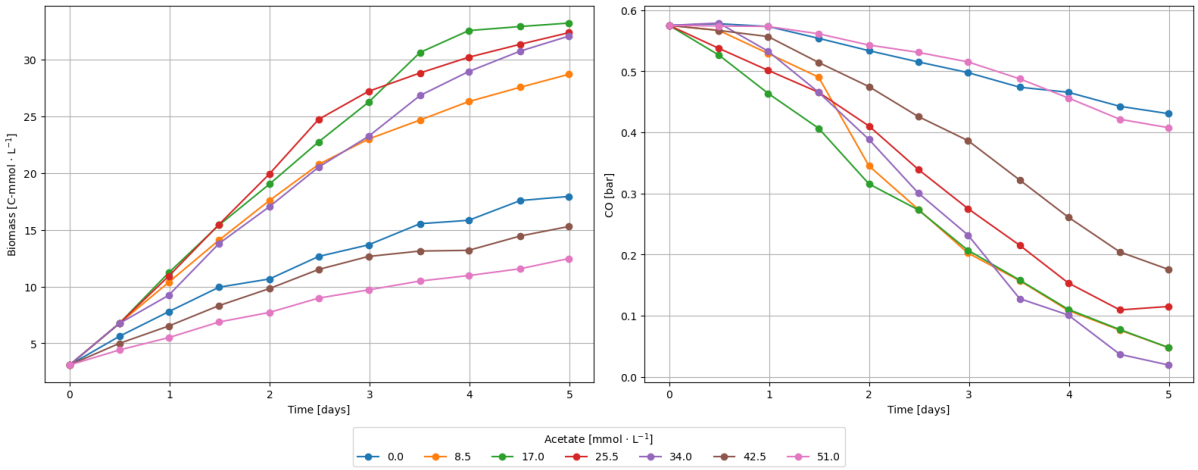

Figure 3: Effect of different initial acetate concentartions with a constant initial 0.6 bar CO partial pressure on *R rubrum* growth

2.3.2. Syngas and CO

Syngas is a widely available waste product mainly composed of CO, CO_2 and H_2 gases, typically produced by gasifying organic waste. Cultivation of *R rubrum* using syngas has been investigated in detail, primarily in relation to sustainable plastic and hydrogen production. The different metabolic pathways operating during syngas fermentation that lead to PHA production were studied by Revelles et al. [16]. In relation to hydrogen production, Najafpour et al. [20] explored the possibility of describing the process using mathematical models, while Klasson et al. [21] examined the potential of employing

[2]With the exception of the data from Godoy et al. [4], which was kindly provided by the authors, all other data in Section 2.3 was extracted from the referenced studies using https://www.graphreader.com/v2.

a mixed culture of *R. rubrum*, *M. barkeri*, and *M. formicicum* to produce methane from syngas in two steps.

A study by Do et al. [22] compared the growth of *R. rubrum* on artificial syngas produced by mixing pure gases with syngas derived from the gasification of corn seed. It was observed that some volatile organic compounds present in real syngas have an inhibitory effect on CO oxidation, which should be considered in potential industrial applications. No detailed studies examining the effect of specific gas ratios of CO, H_2, CO_2 were found. The closest is the study by Karmann et al. [8], who investigated the effect of supplementing syngas composed of 40% CO, 40% H_2, 10% CO_2, and 10% N_2, which was then diluted with varying amounts of pure nitrogen.

To simplify the analysis, the focus of this work was on using a pure CO-N_2 gas mixture in the reactor[3], with CO_2 and H_2 only becoming available through bacterial activity. This occurs via the enzyme carbon monoxide dehydrogenase [8], which catalyzes the water–gas shift reaction shown in Equation 7.

$$CO + H_2O \rightleftharpoons CO_2 + H_2 \tag{7}$$

Based on the available experimental data collected by Godoy et al. [4] using pure CO-N_2 mixtures, different CO concentrations can have three distinct effects: substrate limitation, substrate inhibition, and variations in lag phase length. The variation in lag phase cannot be attributed to inhibition, as this would imply that during the lag phase the concentration of the inhibiting compound, in this case CO, decreases until it no longer inhibits growth. However, this is not observed experimentally, as shown in Figure 2. Biomass growth and the varying lag phases at different CO partial pressures are presented in in Figure 4.

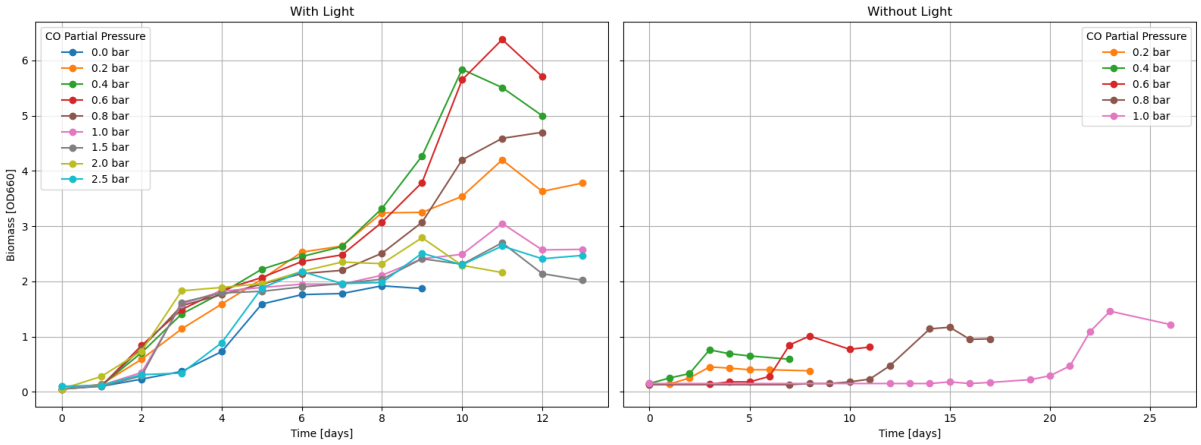

Figure 4: Growth at different CO partial pressures under light (L2 state) and under dark conditions (D1 state) from the study by Godoy et al. [4]

[3]Nitrogen is assumed to be an inert gas in this system since ammonium is supplied in excess, preventing nitrogen fixation.

2.3.3. Light Intensities

The already mentioned study by Bayon-Vincente et al. [18] hypothesized that PHA production may serve as a mechanism for *R. rubrum* to adapt to high light stress and the resulting redox imbalance. The authors also noted the established relationship between bicarbonate consumption during anaerobic growth and the assimilation of organic acids such as acetate, propionate, and butyrate. Furthermore, they suggested that the presence of buffers such as HCO_3^- may allow greater tolerance to high light intensity conditions.

Uffen [23] investigated the transition of *R. rubrum* from high to low light intensity under anaerobic photosynthetic conditions. After the light intensity was reduced, the growth rate declined markedly. After approximately ten generations, once a new stable state with higher pigment content had been established, the growth rate partially recovered.

To date, no studies have systematically examined the effect of different light intensities on the growth of *R. rubrum* in a pure culture. Cerruti et al. [24] investigated the effect of light intensity on mixed cultures of purple phototrophic bacteria (*Blastochloris*, *Rhodobacter*, *Rhodopseudomonas*, and *Thiobaca*) and extrapolated from their data that the maximum growth rate occurred at around 450 W/m², with *Rhodopseudomonas* outperforming the other species under high irradiation. Ross et al. [25] studied the growth of a pure *Rhodopseudomonas palustris* culture in a tubular photobioreactor and observed similar results to Cerruti's, with strong growth inhibition below 200 W/m² and photoinhibition above 600 W/m². The reactor operated under anaerobic conditions with glycerol as the carbon source.

2.4. Existing Models

Several studies have attempted to describe the growth of *R. rubrum* mathematically. Most models address only a single set of environmental conditions, although in recent years a few more comprehensive approaches have been developed.

Segura et al. [26] proposed a dynamic model that predicts changes in the concentrations of VFAs (acetate, propionate, butyrate, and valerate) and the resulting composition of produced PHA monomers under photoheterotrophic conditions. The model also accounts for substrate inhibition and introduces limitation and inhibition factors using the Monod–Ierusalimsky equation (Equation 2).

Cornet et al. [27] developed a framework that simulates biomass composition, productivity, and stability in a continuous cylindrical photobioreactor at light intensities between 50 and 400 W/m². It describes the stoichiometry of biomass and PHB production as functions of light intensity and residence time.

Alloul et al. [28] designed a model to predict and control microbial selection in open raceway reactors used for wastewater treatment. Unlike the previous models that describe pure cultures, this one focuses on competition between PPB (not just *R. rubrum*) and aerobic or anaerobic heterotrophs under varying light and oxygen concentrations. The model includes photoheterotrophic, aerobic chemoheterotrophic, and anaerobic chemoheterotrophic modes, but does not differentiate between more specific metabolic states such as photoorganoheterotrophy, photolithoheterotrophy, and photolithoautotrophy.

3. Materials and Methods

This section presents the experimental setup that is later used to validate the mathematical model described in Section 4.

3.1. Strain and Medium

The medium was prepared based on the RRNCO medium recipe by Kerby et al. [6], with minor modifications. Ferric chloride replaced ferric citrate, and HEPES was used as the buffering agent instead of MOPS. The original recipe does not specify the source of potassium because it relies on a premade solution, in this preparation, a mixture of mono- and dipotassium salts was used. In the past it has also been shown that biotin has no significant impact on growth[4], therefore, it was also omitted.

Table 5: Medium composition

Component	Chemical formula	[mg/L]	[g COD/L]
Sodium acetate trihydrate	$CH_3COONa \cdot 3H_2O$	1360	0.6
Boric acid	H_3BO_3	2.8	
Ethylenediaminetetraacetic acid	Na_2EDTA	20	
Ferric chloride hexahydrate	$FeCl_3 \cdot 6H_2O$	3.2	
Sodium molybdate	Na_2MoO_4	1	
Magnesium sulphate heptahydrate	$MgSO_4 \cdot 7H_2O$	250	
Calcium chloride dihydrate	$CaCl_2 \cdot 2H_2O$	132	
Ammonium chloride	NH_4Cl	1000	
Nickel chloride	$NiCl_2$	0.5	
Sodium sulfide nonahydrate	$Na_2S \cdot 9H_2O$	1	
Sodium bicarbonate	$NaHCO_3$	10.5	
Monopotassium phosphate	KH_2PO_4	6	
Dipotassium phosphate	K_2HPO_4	9	
HEPES		2400	
Yeast extract		1000	1.42 [29]

The pH was adjusted to an initial 7.1 using NaOH and HCl.

For bioreactor inoculation, the *R. rubrum* S1H strain was used, stored in MELiSSA medium at 4 °C.

3.2. Reactor Setup and Lighting

As a batch bioreactor, a 1 L serum bottle, which if fact, has a total volume of 1.15 L, was utilized. The bottle was filled with 0.5 L of medium, leaving a 0.65 L headspace that was filled with an CO - N_2 gas mixture. Samples were collected through two designated ports: one equipped with an internal tube extending to the bottom of the bottle and an external valve for sampling the liquid medium, and another fitted with a one-way valve without an internal tube, enabling direct sampling of the headspace gas phase.The heating plates used were difficult to adjust to an exact temperature but were maintained between 35 and 40 °C.

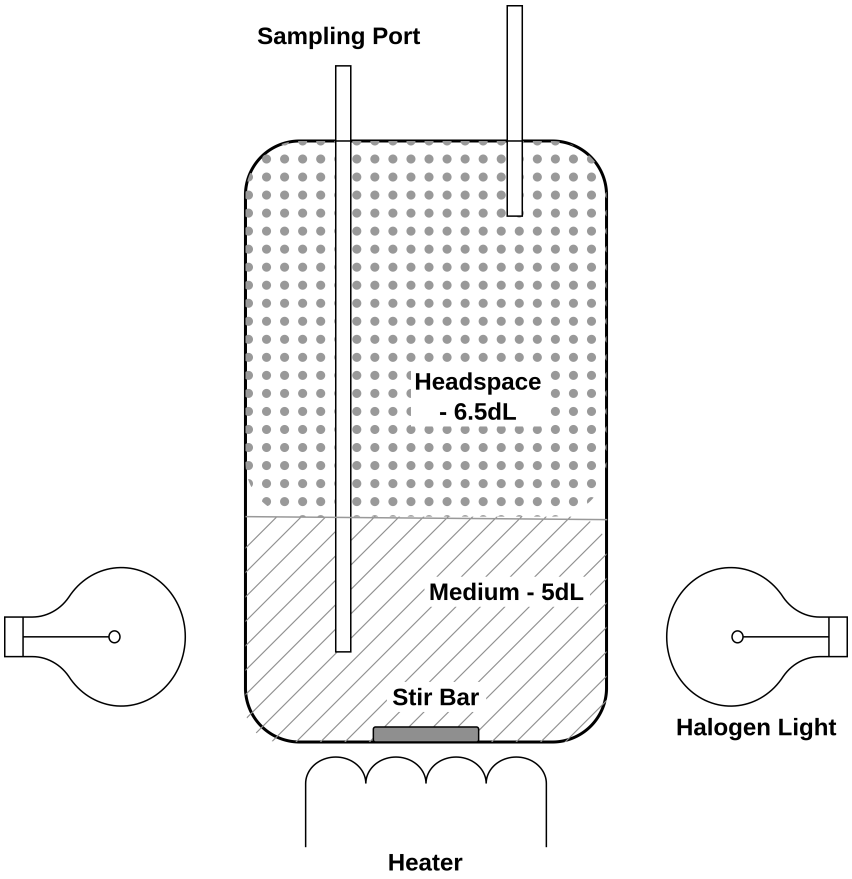

Figure 5: Reactor setup

The lights were positioned on opposite sides of the bioreactor, as shown in Figure 6. To calculate the average irradiance within the reactor, multiple appoaches can be taken. While the commonly used Beer–Lambert law would only require momentary absorbance values at a single wavelength, in this case 660 nm, it would require an attenuation coefficients specifically fitted to *R. rubrum* biomass for each metabolic mode. Given that the attenuation coefficent is unknown, the momentary irradiation is instead calculated from the absorbance measured across all biologically relevant wavelengths, ranging from 400 to 1000 nm, as well as the irradiation spectrum of the light source over the same range.

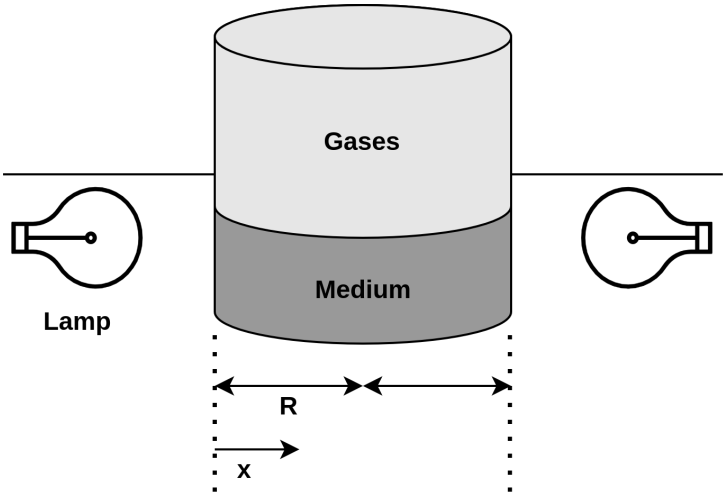

Figure 6: Lighting Setup

Two 20W, 12V GU4 halogen light bulbs were used as the light source, they were filtered through Infra Red 962 3mm Black Perspex Acrylic sheets. Figure 7 shows a picture of the actual setup. Based on these two lights, the discretized equation for calculating the average irradiance is given in Equation 8. Irradiance was measured directly at the glass whole of the reactor, and thus the filtering effect of the acrylic sheets are already included.

$$Irr \approx \frac{1}{2R} \sum_{x=0}^{2r} \left[\sum_{\lambda=400}^{1000} \left(Irr_0(\lambda) \cdot 10^{-A(\lambda) \cdot x} + Irr_0(\lambda) \cdot 10^{-A(\lambda) \cdot (2r-x)} \right) \cdot \Delta\lambda \right] \cdot \Delta x \tag{8}$$

Where Irr represents the average irradiance across the reactor, x denotes the discretized spatial positions within the reactor, r is the radius of the reactor, λ refers to the discretized wavelengths or wavelength ranges, and Irr_0 is the spectral irradiance function at each wavelength.

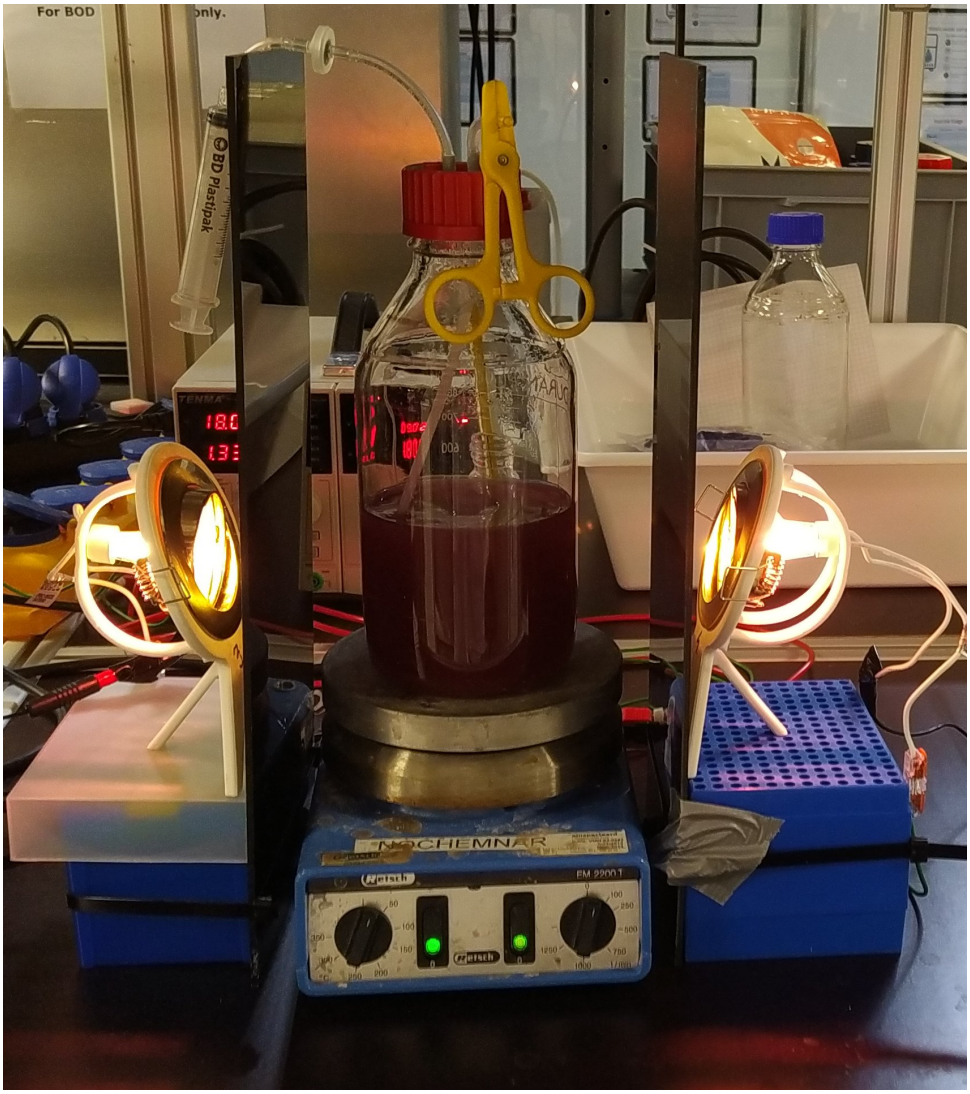

Figure 7: Picture of the photobioreactor

3.3. Analytical Methods

To monitor the state of the microbial growth and the concentrations of the relevant substrates, the following parameters were periodically measured:

- Acetate concentration in the medium: measured daily using gas chromatography
- Partial pressures of gases in the headspace: including CO, CO_2, H_2 measured daily via gas chromatography
- Biomass concentration: measured daily by spectrophotometric absorbance at 660 nm (full absorbance spectra collected between 400–1000 nm) and by VSS measurements
- Light: average light intensity was measured twice a week to acount for potential bulb aging effects

4. Matematical Model

The goal of developing the mathematical model is to predict the future growth of *R. rubrum* and the changes in the concentrations of acetate, CO_2 and H_2, as functions of the initial environmental conditions. It is also essential that the model accurately identifies the active metabolic state at any given time based on the prevailing conditions and reliably predicts the duration of lag phases that occur during transitions between states. If these criteria are met, the model can serve as a valuable tool for process optimization.

4.1. Dealing with Different Metabolic Modes

In Section 2.2, a metabolic classification was established to facilitate the division of the growth phases of *R. rubrum*. This section examines the sequence and interrelationship of these metabolic states as they may occur in a batch reactor, where light is the sole manually controlled variable.

It is assumed that the metabolic activity of PPB alternates only between anaerobic photosynthesis and anaerobic respiration. If conditions are not addequate for either, no microbial growth is assumed with a steady biomass decay rate.

Figure 8 illustrates the possible transitions between metabolic states. Black arrows represent spontaneous transitions, typically caused by substrate depletion, while red arrows indicate transitions requiring manual switching of the light on or off. States with solid borders correspond to the “real” metabolic states, already presented, where growth is possible. States with dashed borders represent no growth. No growth can fall into two categories: a transitional state in which *R. rubrum* cannot utilize the available substrates in the dark, but could resume growth if the light was switched on. The alternative is a terminal states that denote conditions where growth is not possible even with illumination.

If the reactor starts with the light on and only acetate available, the model assumes state L1, where growth continues until acetate is fully consumed. At that point, the system transitions to the terminal state T1, where the CO_2 produced during the L1 phase is still available, but by itself is insufficent to support further growth.

When the reactor is initially under light with both acetate and CO available, it is in state L2. If acetate is depleted before CO drops below the inhibition threshold, the system transitions to terminal state T2, where growth is inhibited. Alternatively, if acetate and CO are depleted simultaneously, the system briefly enters state L1* to consume residual acetate before transitioning to state L3, where growth can continue utilizing the CO_2 and H_2 produced, without CO inhibition. Growth ceases once either H_2 or CO_2 is exhausted, resulting in terminal state T3.

If the reactor starts in the dark with both acetate and CO available, the system begins in state D1. Should acetate be depleted first while CO remains above the inhibition threshold, the system transitions to terminal state T2. If CO is depleted before acetate, the system enters a temporary D0_L1* state where no growth occurs, but switching on the light allows it to progress to state L1* and resume growth from there. Finally, if acetate and CO are depleted simultaneously, the system reaches a temporary D0_L3

state, from which turning on the light enables a direct transition to state L3, again allowing growth to continue.

Naturally, this model is intended to enable growth predictions and does not necessarily the full biological reality.

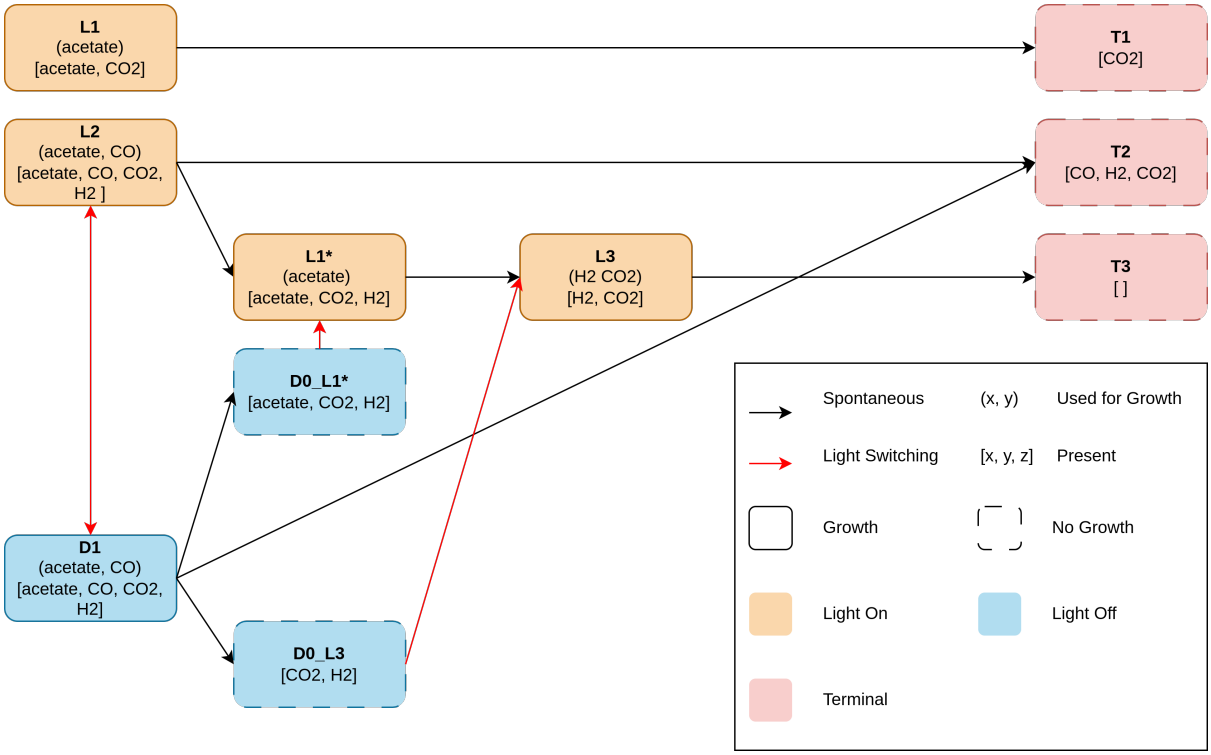

Figure 8: Flow chart of the different metabolic states

The model applies rules, summarized in Equation 9, to determine its current state, designed in a way that no more than one metabolic state can be true at any given time. Where $\theta_{ACE}, \theta_{CO}, \theta_{CO_2}, \theta_{H_2}$, are the minimum concentration values for dissolved concentration above which the system considers the given compound available for growth. θ_{CO}^{cut} is the the cutoff concentration value, above which CO inhibits growth on CO_2 and H_2 in the L3 state. θ_{Irr} is the irradiation cutfoff value that decides whether the system is in dark or under light.

$$
\begin{aligned}
&\text{L1}: \quad C_{ACE} \geq \theta_{ACE} \text{ and } C_{CO} < \theta_{CO} \text{ and } Irr \geq \theta_{Irr} \\
&\text{L2}: \quad C_{ACE} \geq \theta_{ACE} \text{ and } C_{CO} \geq \theta_{CO} \text{ and } Irr \geq \theta_{Irr} \\
&\text{L3}: \quad C_{ACE} < \theta_{ACE} \text{ and } C_{CO} < \theta_{CO}^{cut} \text{ and } C_{CO_2} \geq \theta_{CO_2} \text{ and } C_{H_2} \geq \theta_{H_2} \text{ and } Irr \geq \theta_{Irr} \\
&\text{D1}: \quad C_{ACE} \geq \theta_{ACE} \text{ and } C_{CO} \geq \theta_{CO} \text{ and } Irr < \theta_{Irr}
\end{aligned}
\tag{9}
$$

As it can be seen from these logic rules, the implement the computational model does not have memory to store the sequence of the previous states, and hence does not differentiate between states as defined in the flowchart. For example L1 and L1*, both are classified as L1, or the temporary no growth states of D0_L1*, D0_L3, and terminal states T1, T2, T3, all of which are classifed as “No

Growth" state. The main advantage of defining these somewhat fictious transitional states is that they later facilitate the interpretation of certain model behaviors. For instance, in Figure 9, which shows an output of the implemented model, these states help verify whether the observed sequence of metabolic states is feasible.

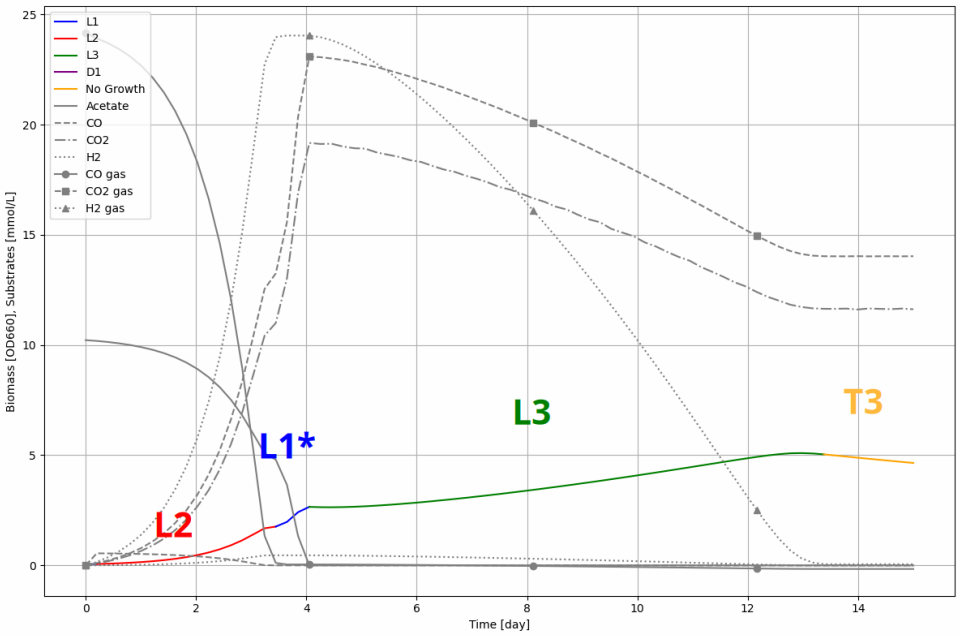

Figure 9: An example output of the computational model. The exact states, as defined in the flowchart, were manually labeled.

4.2. Substrate Limitation and Inhibition

In Section 2.3, the main effects of key model parameters influencing *R. rubrum* growth were presented. The focus was on the different substrates utilized in the investigated metabolic states and illumination, based on the available published research. In this section, the previously presented data are used to estimate certain model coefficients.

4.2.1. Effect of Different Acetate Concentrations

Figure 3 showed the relationship between the initial acetate concentrations and the observed growth rates based on the data collected by Ghasem et al. [17]. Now, three of the unstructured models presented in Table 3, namely the Monod-Ierusalimsky, Haldane, and Aiba models (Equation 2, 3, 4 respectively), are fitted to the extracted maximum specific growth rate values of the same data set for each initial acetate concentration [4]. The results are shown in Figure 10.

For the model fitting, μ_{max} had to be constrained to a somewhat arbitrary 1.5 day^{-1}, about 20% higher than the maximum observed growth rate, as leaving it unconstrained resulted in an almost perfect fit

[4]The first entry for the no-acetate case was removed, as the absence of acetate would indicate photoautotrophic growth rather than the photoheterotrophic growth, here classified as L2. It is interesting to note that in other studies [4], no growth was observed at all without acetate. See Figure 2, specifically the "Light - CO at 2 bar" plot, where growth ceases after acetate is depleted.

at around μ_{max} = 8 day^{-1}. This was considered unrealistic and likely significantly overfitted, mainly due to the limited data available, particularly at low acetate concentrations. The highest maximum growth rate was observed at 18 mmol · L^{-1} acetate concentration.

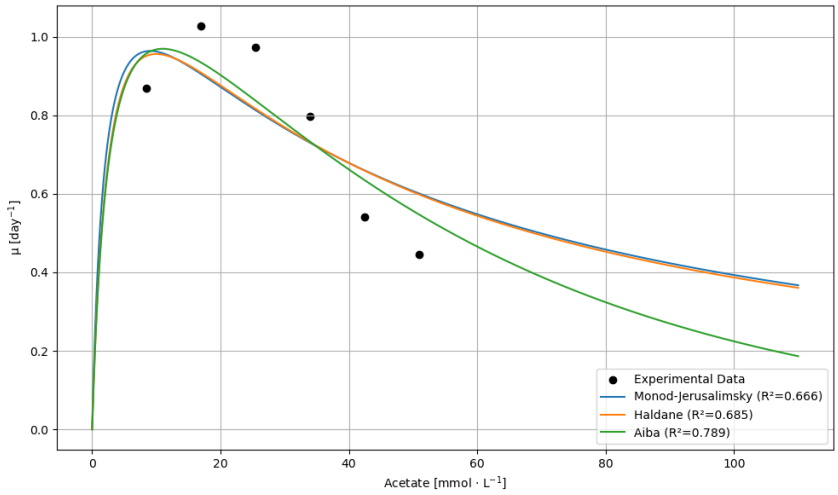

Figure 10: Effect of different initial acetate concentrations on the maximum growth rate

The parameters of the fitted models can be seen in Table 6. Overall, Aiba's model provided the best fit.

Table 6: Parameters of the different growth models fitted to describe the relationship between acetate concentrations and growth rates, in L2 state, under light conditions with available CO

Model	μ_{max}^{L2}	$K_{s,ACE}^{L2}$	$K_{i,ACE}^{L2}$	R^2
Monod-Jerusalimsky	1.5	2.239184	36.616853	0.666135
Haldane	1.5	2.837170	35.106506	0.684548
Aiba	1.5	2.850136	53.412072	0.788994

4.2.2. Effect of Different CO Concentrations

As stated CO concentrations had three different type of effect on *R. rubrum*: substrate limitation, inhibition and lag phase length change. In this sub-chapter the first two of these effect is invesigated under both dark and light conditions, states L2 and D1, with acetate and CO available. Data presented on Figure 4, collected by Godoy et al. [4] is used.

Under Light Conditions - L2

The same three models as before, Equation 2, 3, 4, were applied to the available data. The case with no CO provided was removed, as this represents a different state, L1[5]. In cases with CO partial pressures

[5] L1 is photoorganoheterotrophy, photosynthesis with only acetate available, while L2 is chotolithoheterotrophy with CO as electron donor and acetate as carbon source.

between 0.2 bar and 1 bar, as previously noted, a second growth phasestate L3 occurs, but it does not influences the maxium growth rate[6].

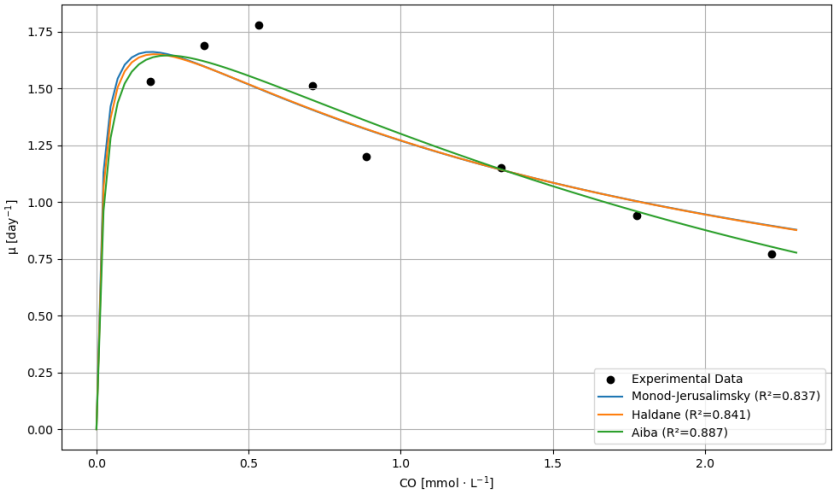

Figure 11: Effect of different initial CO concentrations on the growth rates in state L2

During the model fitting, the the μ_{max} value, as before, had an upper bundary set to 2 day^{-1}, to avoid overfitting. All CO values expressed in the study as bar partial pressures were converted to mmol · L^{-1} dissolved in the medium, assuming 30°C and saturation, with no growth limitation by slow dissolution rate.

Table 7: Parameters of the different growth models fitted to describe the relationship between CO concentrations and growth rates under light conditions

Model	μ_{max}^{L2}	$K_{s,CO}^{L2}$	$K_{i,CO}^{L2}$	R^2
Monod-Jerusalimsky	2	0.017311	1.824217	0.837016
Haldane	2	0.020261	1.806859	0.841138
Aiba	2	0.024667	2.460851	0.887359

Dark Conditions - D1

For the dark condtions, the same steps were taken as for light one. First the already presented three growth models were fitted to the experimental data from the study by Godoy et al.[4], as shown in Figure 12.

[6]The presence of L3 state does not interfere with using the data to investigate the maximum growth rate of L2, as in all cases the highest growth rate occurred during the L2 phase.

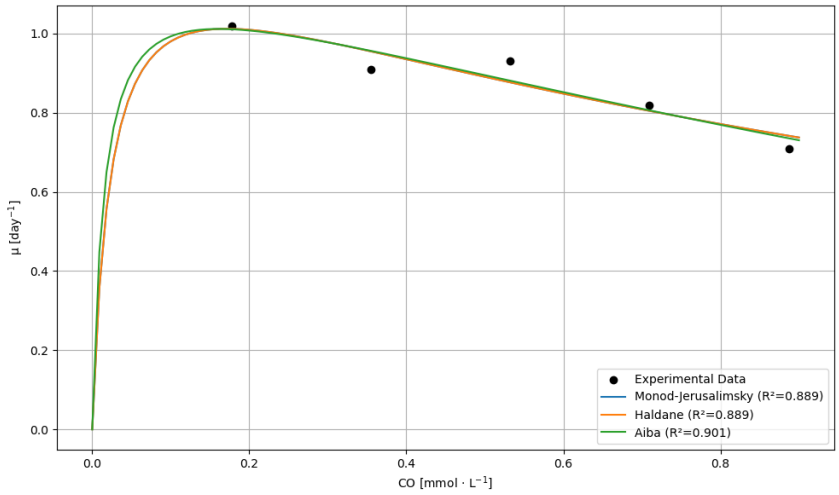

Figure 12: Effect of different initial CO concentrations on the growth rates in darkness in state D1

This time, there was no need for establishing upper boundaries for possible μ_{max} values to avoid overfitting, as the best fit was achived by 1.2 day^{-1}, which is completly realistic. The three different growth models performed almost identiacally as shown in Table 8.

Table 8: Parameters of the different growth models fitted to describe the relationship between CO concentrations and growth rates under dark conditions

Model	μ_{max}^{D1}	$K_{s,CO}^{D1}$	$K_{i,CO}^{D1}$	R^2
Monod-Jerusalimsky	1.318469	0.024245	1.214974	0.888873
Haldane	1.292677	0.023771	1.239220	0.888873
Aiba	1.208838	0.015302	1.849109	0.901353

4.2.3. Effects of Different Light Intensities

Since the exact relationship between the growth rate of *R. rubrum* and light intensity has not yet been studied in detail directly, data from the study by Ross et al. [25], presented earlier in Section 2.3.3, describing the relationship between light intensity and *Rhodopseudomonas growth*, are used as a proxy.

As before, the models, Equation 2, 3, 4, were fitted to the experimental data from the study, shown in Figure 13.

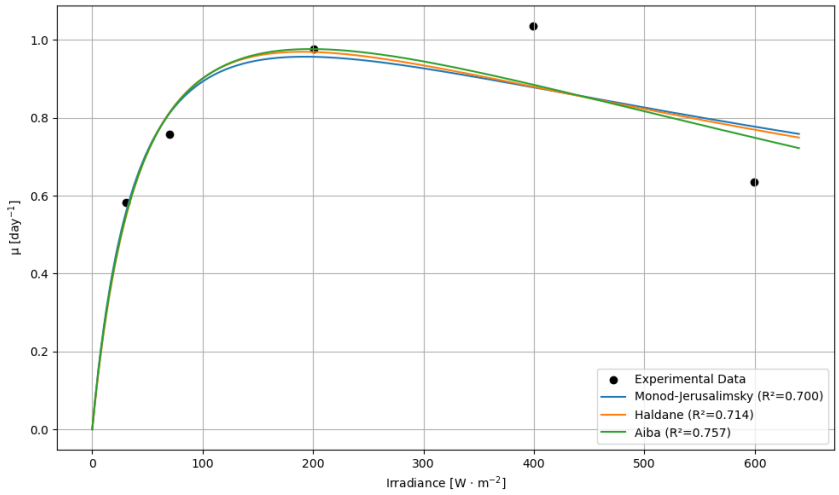

Figure 13: Specific growth rate of *Rhodopseudomonas palustris* as function of irradiance from the study done by Ross et al.[25]

The maximum growth rate was bounded at a 1.5 day^{-1} again to avoid overfitting.

Table 9: Parameters of the fitted growth models for different irradiance levels

Model	μ_{max}	K_s	K_i	R^2
Monod-Jerusalimsky	1.5	48.455595	764.124656	0.700162
Haldane	1.5	51.969675	695.639110	0.713733
Aiba	1.5	50.255411	977.011214	0.756904

4.3. Lag Phases

4.3.1. Lag Phase Parameters

To investigate the relationship between CO concentrations and the length of lag phases in states L2 and D1, three different expressions, Equation 10, 11, 12, were tested[7].

First Order:

$$Lag = k \cdot C_{CO} \tag{10}$$

Second Order:

$$Lag = k \cdot C_{CO}^2 \tag{11}$$

[7]Originally, an additional $+\alpha$ parameter was included at the end of all three expressions to allow a vertical offset for better fits. However, it was not needed, as in both light and dark cases, the best fits were obtained with zero or near-zero α values.

Exponential:

$$Lag = k \cdot \exp(\beta \cdot C_{CO}) \tag{12}$$

Under Light Conditions - L2

The expressions describing the different possible relationships between dissolved CO concentrations was fitted to the light case of the experimental data of Godoy et al.[4], shown in Figure 14.

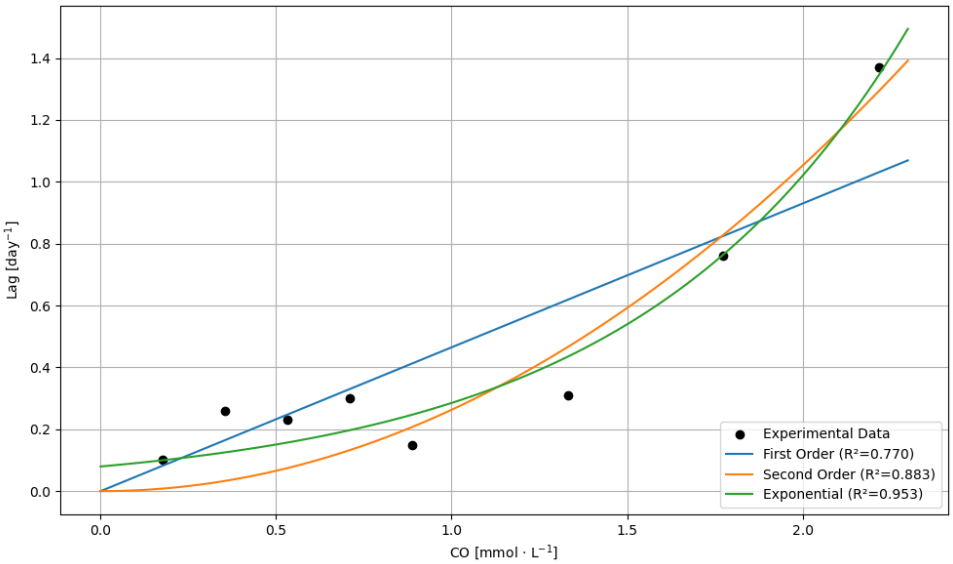

Figure 14: Effect of different CO concentrations on the length of the lag phase in state L2

The parameters of the fitted experessions are shown in Table 10. Both the second order and the exponential expression provides a good fit to the experimental data, although the former only needs one, while the latter two parameters fitted.

Table 10: Parameter of the different expressions aiming to describe the relationship between lag phase length and CO concentrations, under light, in L2 state

Model	k^{L2}	β^{L2}	R^2
First order	0.464866	-	0.770475
Second order	0.263050	-	0.882740
Exponential	0.079721	1.274285	0.953441

Dark Conditions - D1

The same steps as for the light case was done for the dark, shown in Figure 15.

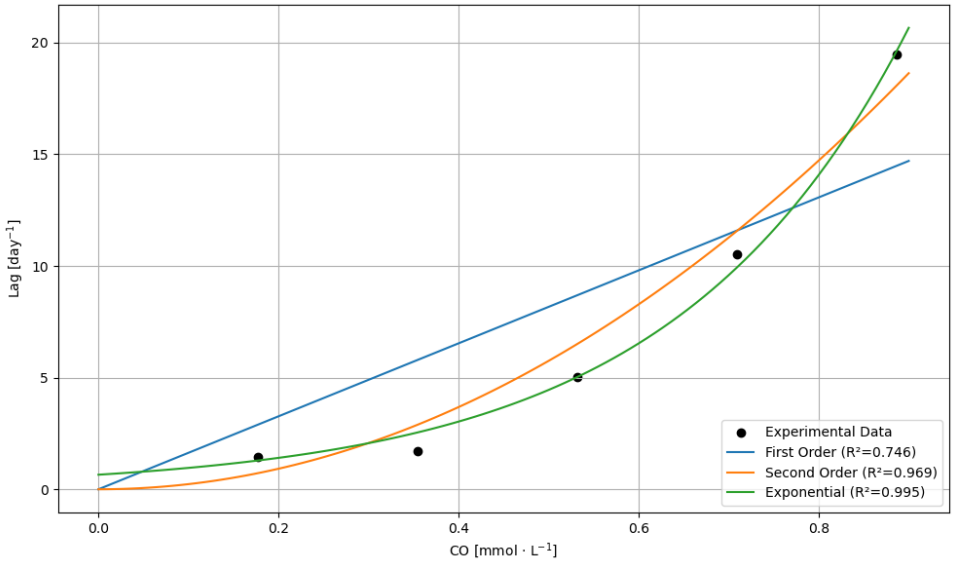

Figure 15: Effect of different CO concentrations on the length of the lag phase in darkness, in state D1

Both the second-order and exponential expressions describing lag phase lengths again provided a good fit to the experimental data from the study, show in Table 11.

Table 11: Parameter of the different expressions aiming to describe the relationship between lag phase length and CO concentrations, under darkness, in D1 state

Model	k^{D1}	β^{D1}	R^2
First order	16.336231	-	0.745516
Second order	23.000268	-	0.968909
Exponential	0.652559	3.839064	0.995233

4.3.2. Lag Phase Functions

In the model, when a metabolic state is inactive or in its lag phase, its growth rate is set to zero. Determining whether a specific metabolic state is active follows the procedure described in Section 4.1. Once a state is identified as active, the model distinguishes between the lag phase and the growth phase using the lag phase functions. These functions are represented by Heaviside step functions that take a value of zero until a defined period has elapsed after the condition for the given metabolic state, defined in Equation 9, first becomes true. The duration of the lag phase is either a constant τ, based on the values reported by Godoy et al. [4], or a function of the CO concentration, as described by the exponential relationship introduced earlier in this section. After this period, the function value changes to one. The model assumes that each metabolic mode occurs only once during a run cycle or, if interrupted, only for a short period. Brief interruptions, for example those caused by low volumetric mass transfer rates, are not assumed to reset the lag phase. The lag phase functions are described by Equation 13, 14, 15, 16 .

$$H_{L1}(t) := \begin{cases} 1, & t \geq \tau_{L1} + t_{0,L1} \\ 0, & t < 0 \end{cases} \tag{13}$$

$$H_{L2}(t) := \begin{cases} 1, & t \geq k_{L2} \cdot \exp(\beta_{L2} \cdot C_{CO}) + t_{0,L2} \\ 0, & t < 0 \end{cases} \tag{14}$$

$$H_{L3}(t) := \begin{cases} 1, & t \geq \tau_{L3} + t_{0,L3} \\ 0, & t < 0 \end{cases} \tag{15}$$

$$H_{D1}(t) := \begin{cases} 1, & t \geq k_{D1} \cdot \exp(\beta_{D1} \cdot C_{CO}) + t_{0,D1} \\ 0, & t < 0 \end{cases} \tag{16}$$

Where t_0 values are the first time when the coditions for a given metabolic state became true.

4.4. Growth Rates

The growth rate for each metabolic state is defined using logic statements. As previously noted, at any given time, no more than one metabolic state can be active, all others are false, resulting in zero growth rate in those. When the logical condition for a specific metabolic state is true, and the lag phase has passed, its growth rate is assumed to be limited by the concentrations of its substrates, acetate and light for L1, acetate, CO, and light for L2, CO_2, H_2 and light for L3, and acetate and CO for D1. Inhibition effects, as discussed in Section 4.2.1 and Section 4.2.2, were incorporated for acetate, CO, and irradiation by extending the Monod model to the Aiba formulation through the inclusion of an exponential multiplier. The inhibitory effects of acetate for L1 and D1 states, and CO_2 and H_2 for L3 were not considered due to insufficient literature to characterize them. The lag function H_i, aimed to simulate the time needed for the bacetria to aclimatize itself for the new envrionmental conditions, can either take the value of zero or one, see Section 4.3

If L1 is true:

$$\mu_{L1} = \mu_{L1}^{\max} \cdot \frac{C_{ACE}}{C_{ACE} + K_{s,ACE}^{L1}} \cdot \frac{Irr}{Irr + K_{s,Irr}^{L1}} \cdot \exp\left(\frac{-Irr}{K_{i,Irr}^{L1}}\right) \cdot H_{L1}(t) \tag{17}$$

Otherwise: $\mu_{L1} = 0$

If L2 is true:

$$\mu_{L2} = \mu_{L2}^{\max} \cdot \frac{C_{ACE}}{C_{ACE} + K_{s,ACE}^{L2}} \cdot \frac{C_{CO}}{C_{CO} + K_{s,CO}^{L2}} \cdot \frac{Irr}{Irr + K_{s,Irr}^{L2}} \cdot \exp\left(\frac{-C_{ACE}}{K_{i,ACE}^{L2}} + \frac{-C_{CO}}{K_{i,CO}^{L2}} + \frac{-Irr}{K_{i,Irr}^{L2}}\right) \cdot H_{L2}(t) \tag{18}$$

Otherwise: $\mu_{L2} = 0$

If L3 is true:

$$\mu_{L3} = \mu_{L3}^{\max} \cdot \frac{C_{CO_2}}{C_{CO_2} + K_{s,CO_2}^{L3}} \cdot \frac{C_{H_2}}{C_{H_2} + K_{s,H_2}^{L3}} \cdot \frac{Irr}{Irr + K_{s,Irr}^{L3}} \cdot \exp\left(\frac{-Irr}{K_{i,Irr}^{L3}}\right) \cdot H_{L3}(t) \tag{19}$$

Otherwise: $\mu_{L3} = 0$

If D1 is true:

$$\mu_{D1} = \mu_{D1}^{\max} \cdot \frac{C_{ACE}}{C_{ACE} + K_{s,ACE}^{D1}} \cdot \frac{C_{CO}}{C_{CO} + K_{s,CO}^{D1}} \cdot \exp\left(\frac{-C_{CO}}{K_{i,CO}^{D1}}\right) \cdot H_{D1}(t) \tag{20}$$

Otherwise: $\mu_{D1} = 0$

4.4.1. OD660, Biomass and Yields

Most existing studies do not provide continuous biomass concentration data that could be used to calculate yields, in terms of consumption or production per unit biomass change. If the storage polymer concentrations are negligible, it can be assumed that volatile suspended solids (VSS) and biomass are equivalent.

Studies by Cerruti et al. [30] and Godoy et al. [4] include data on the relationship between absorbance at 660 nm (OD660) and VSS. Cerruti's study compares OD660 and VSS values, showing a linear relationship between them, while Godoy's study provides a set of VSS–OD660 value pairs for both dark and light runs, at the end of the reactor run of a series of different dark and light reactor experiments.

Figure 16 shows the three data sets with fitted lines. The large discrepancy between the slopes of the fitted lines of Cerruti's data, Godoy's dark data set, and Godoy's light data set may be explained by the fact that the latter was fitted at higher concentrations only, where the linear relationship may no longer hold.

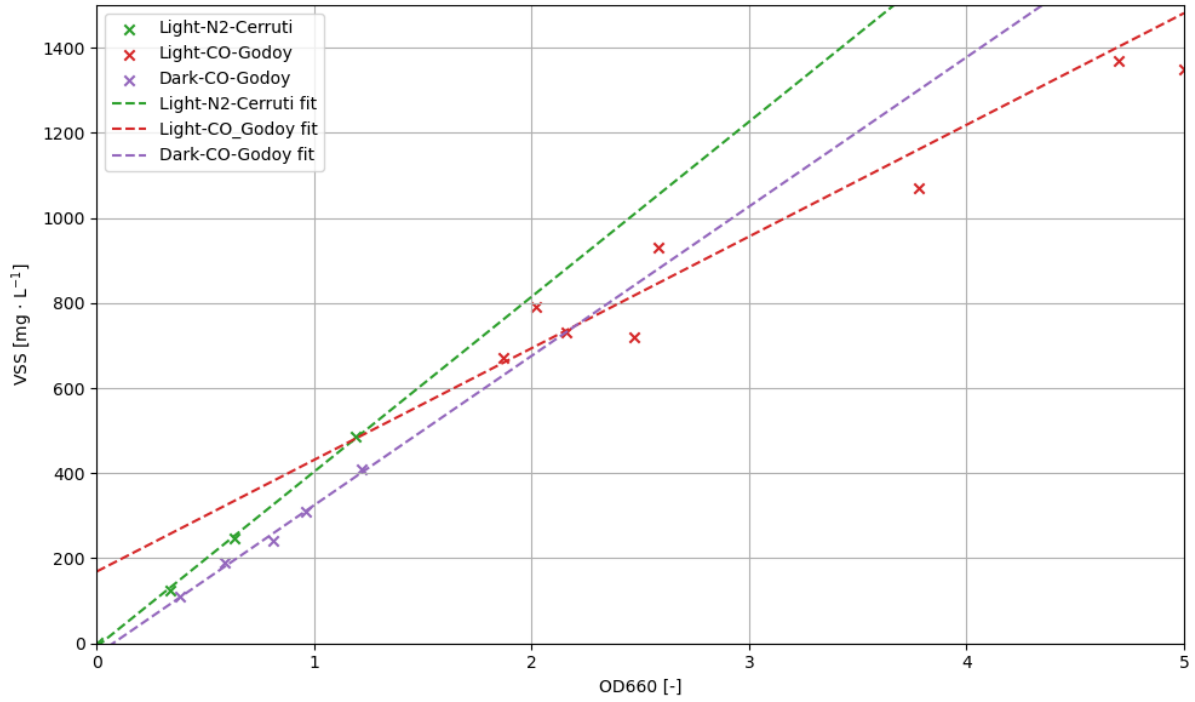

Figure 16: Relationship between absorbance at 660 nm and volatile suspended solids concentrations for the three data sets

When the OD660 value is zero, it is logically assumed that the VSS concentration is also zero. Since the line fitted to Cerruti's data is the closest to the origin, it can be considered the best approximation, at least for lower concentrations. The functions of the fitted lines are shown in Table 12 .

Table 12: Fitted linear function of OD660 versus VSS

Data Set	VSS [mg · L^{-1}]	R^2
Light-N2-Cerruti	411.18 * OD660 - 7.46	0.99
Light-CO-Godoy	262.41 * OD660 + 169.06	0.94
Dark-CO-Godoy	350.90 * OD660 - 25.92	0.99

Using the Light–N2–Cerruti function, VSS values can be generated for the data set presented in Figure 2 from the corresponding OD660 values. These can then be further converted to biomass concentrations, expressed in C-mmol/L, using the average biomass composition of $C_1H_{1.8}O_{0.38}N_{0.18}P_{0.014}$ [12]. Yields can be calculated from the same data set using $Y = \Delta S/\Delta X$. It was found that, instead of calculating yields from the change between two consecutive measurements, using the change over the entire interval of a metabolic state, including the lag phase, provides the most realistic values. The resulting yields for substrates and products of the different metabolic states are presented in Table 13.

Table 13: Yield coefficients for the four metabolic states

Parameter	L1	L2	L3	D1
Y_ACE	-0.33	-0.26	0	-0.36
Y_CO	0	-3.89	-0.22	-8.75
Y_CO2	4.36	2.96	-0.56	7.45
Y_H2	0	3.47	-2.13	8.46

4.5. Mole Balance Equations

Mole balances were formulated for biomass and the potential substrates associated with the four defined metabolic states. It is assumed that ammonium is present in excess in the medium, and nitrogen fixation does not occur. Similarly, phosphate and all other essential nutrients required by *R. rubrum* are considered to be present in excess. Yields were calculated in Section 4.4.1.

Since gases in the bioreactor exist both dissolved in the liquid phase and in the headspace, separate equations are made for CO, CO_2, H_2 in each phase. The corresponding Henry's law constants to calculate their saturation concentration, H^{cc}_{CO}, $H^{cc}_{CO_2}$, $H^{cc}_{H_2}$, are calculated in Section A.2, volumetric mass transfers, kLa_{CO} , kLa_{CO_2} , kLa_{H_2} is caculated in Section A.3.

Biomass:

$$\frac{dX}{dt} = X\left(\mu_{L1} + \mu_{L2} + \mu_{L3} + \mu_{D1} - \mu_d\right) \tag{21}$$

Acetate:

$$\frac{dC_{ACE}}{dt} = X\left(\mu_{L1}Y^{L1}_{ACE} + \mu_{L2}Y^{L2}_{ACE} + \mu_{L3}Y^{L3}_{ACE} + \mu_{D1}Y^{D1}_{ACE}\right) \tag{22}$$

CO (liquid):

$$\frac{dC_{CO}}{dt} = X\left(\mu_{L1}Y^{L1}_{CO} + \mu_{L2}Y^{L2}_{CO} + \mu_{L3}Y^{L3}_{CO} + \mu_{D1}Y^{D1}_{CO}\right) + kLa_{CO}\left(H^{cc}_{CO} \cdot C^{gas}_{CO} - C_{CO}\right) \tag{23}$$

CO (gas):

$$\frac{dC^{gas}_{CO}}{dt} = -kLa_{CO}\left(H^{cc}_{CO} \cdot C^{gas}_{CO} - C_{CO}\right) \cdot \left(\frac{V_{liq}}{V_{gas}}\right) \tag{24}$$

CO_2 (liquid):

$$\frac{dC_{CO_2}}{dt} = X\left(\mu_{L1}Y^{L1}_{CO_2} + \mu_{L2}Y^{L2}_{CO_2} + \mu_{L3}Y^{L3}_{CO_2} + \mu_{D1}Y^{D1}_{CO_2}\right) + kLa_{CO_2}\left(H^{cc}_{CO_2} \cdot C^{gas}_{CO_2} - C_{CO_2}\right)$$

(25)

CO_2 (gas):

$$\frac{dC_{CO_2}^{gas}}{dt} = -kLa_{CO_2}\left(H_{CO_2}^{cc} \cdot C_{CO_2}^{gas} - C_{CO_2}\right) \cdot \left(\frac{V_{liq}}{V_{gas}}\right) \tag{26}$$

H_2 (liquid):

$$\frac{dC_{H_2}}{dt} = X\left(\mu_{L1}Y_{H_2}^{L1} + \mu_{L2}Y_{H_2}^{L2} + \mu_{L3}Y_{H_2}^{L3} + \mu_{D1}Y_{H_2}^{D1}\right) + -kLa_{H_2}\left(H_{H_2}^{cc} \cdot C_{H_2}^{gas} - C_{H_2}\right) \tag{27}$$

H_2 (gas):

$$\frac{dC_{H_2}^{gas}}{dt} = -kLa_{H_2}\left(H_{H_2}^{cc} \cdot C_{H_2}^{gas} - C_{H_2}\right) \cdot \left(\frac{V_{liq}}{V_{gas}}\right) \tag{28}$$

4.6. Model Parameters

Ideally, system identification would involve running a large number of reactors to determine, new precise half-saturation and inhibition coefficients for the specific strain, reactor setup, medium, and lighting conditions. However, this is beyond the scope of the present work. Instead, data from existing literature were used, already presented above. Here, in Table 14 all the different groups of parameters and the source of their assigned values are summarized.

Table 14: The list of parameters of the model

Group	Variable Names	Notes
Maximum Growth Rates:	$\mu_{L1}^{\max}, \mu_{L2}^{\max}, \mu_{L3}^{\max}, \mu_{D1}^{\max}$	These values can be determined by fitting the model to the collected data. However, given that the medium and setup are similar to those used by Godoy et al. [4], it can be assumed that the maximum growth rates are approximately $\mu_{L1}^{\max} =$ 1.5 day^{-1}, $\mu_{L2}^{\max} =$ 2 day^{-1}, $\mu_{L3}^{\max} =$ 1.5 day^{-1}, $\mu_{D1}^{\max} =$ 1.2 day^{-1}

Group	Variable Names	Notes
Half-Saturation Coefficents	$K_{s,ACE}^{L1}$, $K_{s,Irr}^{L1}$, $K_{s,ACE}^{L2}$, $K_{s,CO}^{L2}$, $K_{s,Irr}^{L2}$, K_{s,CO_2}^{L3}, K_{s,H_2}^{L3}, $K_{s,Irr}^{L3}$, $K_{s,ACE}^{D1}$, $K_{s,CO}^{D1}$, $K_{s,Irr}^{D1}$	With the limited literature available, it is assumed for now that the light-related half-saturation and inhibition coefficients ($K_{s,Irr}$, $K_{i,Irr}$) are the same for all metabolic states. Other coefficients for states L2 and D1 have been determined in Section 4.2. For state L1, $K_{s,ACE}^{L1} = 0.05$ mmol/L is used based on [30]. There is insufficient information on K_{s,CO_2}^{L3}, K_{s,H_2}^{L3}, for now, it is assumed that there is a minimum substrate limitation, and they have a value of 0.01 mmol/L.
Inhibition Coefficents	$K_{i,Irr}^{L1}$, $K_{i,ACE}^{L2}$, $K_{i,CO}^{L2}$, $K_{i,Irr}^{L2}$, $K_{i,Irr}^{L3}$, $K_{i,CO}^{D1}$	These coefficients have all been determined in Section 4.2. Inhibitions present in states L1 and L3 were excluded from the growth model due to insufficient data. Unlike half-saturation coefficients, which influence every growth cycle as the corresponding substrate is depleted, inhibition is not always present and would therefore require significantly more data to estimate.
Yield Coefficients:	Y_{ACE}^{L1}, Y_{CO}^{L1}, $Y_{CO_2}^{L1}$, $Y_{H_2}^{L1}$, Y_{ACE}^{L2}, Y_{CO}^{L2}, $Y_{CO_2}^{L2}$, $Y_{H_2}^{L2}$, Y_{ACE}^{L3}, Y_{CO}^{L3}, $Y_{CO_2}^{L3}$, $Y_{H_2}^{L3}$, Y_{ACE}^{D1}, Y_{CO}^{D1}, $Y_{CO_2}^{D1}$, $Y_{H_2}^{D1}$,	Rough yield values for the different metabolic states have been deterimined in Section 4.4.1 .
Delay Coefficents:	τ_{L1}, τ_{L3}, k_{L2}, β_{L2} , k_{D1}, β_{D1}	Delay coefficients for states L2 and D1, as a function of CO concentrations, have been determined in Section 4.2.2. Data are also available for $\tau_{L1} = 0.12$ days and $\tau_{L3} = 0.4$ days [4]. It has to be noted that these constant values are based on single runs from [4], so they might not be very accurate.

Group	Variable Names	Notes
Thresholds:	$\theta_{ACE}, \theta_{CO}, \theta_{CO_2}, \theta_{H_2}, \theta_{CO}^{cut}$	With the exception of θ_{CO}^{cut} , all of these thresholds are used by the model to determine the active metabolic mode at the point where substrate limitation prevents further growth. Therefore, $\theta_{ACE}, \theta_{CO}, \theta_{CO_2}, \theta_{H_2}$ were assigned an arbitrarily low value of $0.1 mmol/L$, serving only to indicate the presence of the substrate in the system. In contrast, θ_{CO}^{cut}has a biological significance, indicating whether the CO concentration is low enough to allow growth on H_2 and CO_2 . Based on literature [4], this value is approximately 0.2 mmol/L.
Death rates:	$d_{default}$	Since in the current model this value is only applied when no growth occurs, it is not very relevant from a modeling perspective. Therefore, for now it is assumed to have a somewhat arbitrary value of 0.3 day.

5. Results & Discussion

5.1. Comparing the Model to Training Data

Approximately two-thirds of the data used in the model were extracted or extrapolated from the time series reported by Godoy et al. [4]. It is therefore reasonable to compare the model with this dataset in order to obtain an initial assessment of its precision and accuracy under optimal conditions. The results of this comparison are shown in Figure 17 .

Out of the few values that were estimated and not the result of model fitting in Table 14, the only necessary adjustments concerned the maximum growth rates. In Section 4.2.1, estimated maximum growth rate were set to approximately 20% higher than the highest measured specific growth rates of their respective study to avoid overfitting. These values were subsequently adjusted to $\mu_{L2}^{\max} = 5$ day^{-1}, $\mu_{L3}^{\max} = 0.15$ day^{-1} during simulation.

As shown in Figure 17, the most obvious discrepancy is that at higher biomass concentrations the model systematically underestimates the observed biomass concentrations. This is assumed to be mainly due to the fact that these biomass concentrations were extrapolated from OD660 values (see Section 4.4.1), where it was noted that the relationship between absorbance and biomass concentration does not appear to remain strictly linear across the full range of concentrations. Another possible contributing factor is that the calculated yields may be systematically higher than in reality, for instance, if they include the effects of unrelated processes occurring either at the beginning or the end of the growth phase in a given metabolic state.

Apart from the absolute biomass concentrations, the shape of the growth curves, the characteristics of the metabolic states, and the lengths of the lag phases are all reasonably close to the measured values. Likewise, the predicted substrate concentrations agree well with the experimental data, with even the largest discrepancies remaining within $\pm 30\%$.

Unfortunately, the approximate nature of the yield values makes the evaluation and sensitivity analysis of the potentially more accurate half-saturation and substrate limitation coefficients impoossible, as their effect compared to the effect of the stoichiometric yields is negligible. As long as their order of magnitude is correct, they do not have a large effect on the model's behavior.

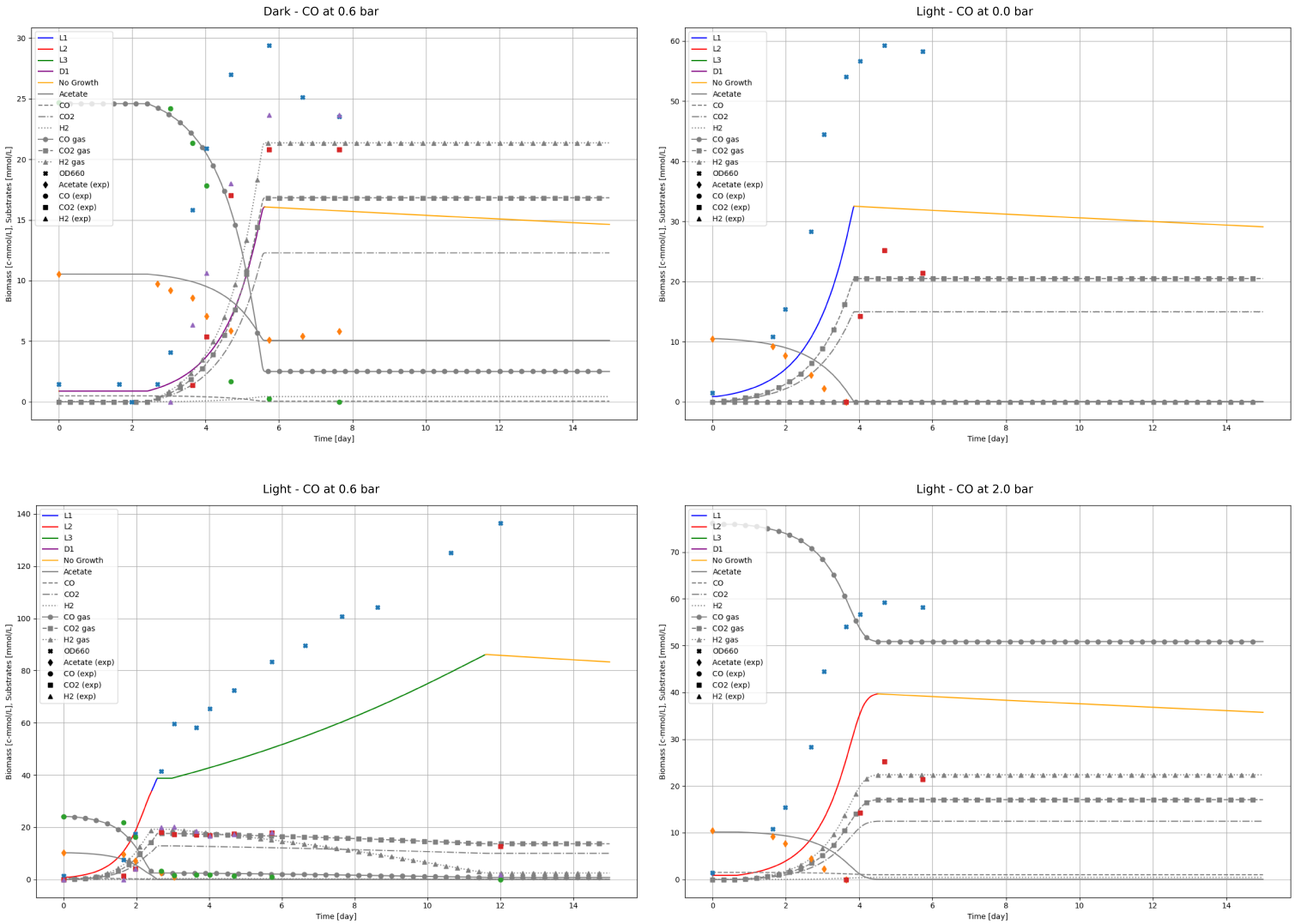

Figure 17: Model compared to the data of the four complete data sets

The big advange of the presented approach is the transparency of the source of different values, which should in principle be reusable in other models. The presented model includes 57 parameters, 49 of which are related to microbial growth. Of these 49, only nine parameters whice were no directly calculated or derived from the literature required adjustment (parameters releated to growth rates and thresholds).

An alternative approach to parameter determination would be to treat either all, or a subset of the parameters as completely unknown, values constrained within predefined realistic intervals, and then fit the model to the available data. However, due to the limited data, many parameters, such as lag phase duration, growth rates, and yields, are difficult to estimate reliably because of their complex interdependencies. While such an approach might yield better predictive results for the training set, its reusability would be limited. By contrast, the model based on individually calculated parameters, although less accurate both with respect to its training data and also possibly to new cases, is overall more flexible. For example, small changes in environmental input parameters are unlikely to affect its predictive performance as significantly.

5.2. Reactor Runs

To assess the potential of the model in describing the behavior of *R. rubrum*, three distinct reactor runs were conducted using the experiment setup presented in Section 3.

All three reactor runs began with medium containing 10–11 mmol/L acetate and approximately 1.3 c-mmol/L biomass extrapolated from the measured OD660 values as described in Section 4.4.1. Two of the three were illuminated with an average of 40 W/m^2 of filtered light. Two of the three, one dark and one light, were supplemented with a 73% CO - 27% N_2 gas mixture, while the third contained only N_2 in the headspace. The results of these runs are shown in Figure 18.

In the ‘Light - CO at 0.0 bar’ run, corresponding to L1 growth on acetate alone, the results behaved as expected. However, a small amount of growth was observed even on day 7, three days after acetate was completely depleted. This may be explained by the presence of residual carbon sources (e.g. succinate from the inoculation medium or starch extract) or by measurement errors, potentially amplified by biomass estimates extrapolated from OD660 values.

In the ‘Light - CO at 0.7 bar’ run, L2 growth on acetate and CO was observed, but the expected subsequent transition to L3 (growth on CO_2 and H_2) did not occur, despite CO concentrations being below inhibitory levels. One possibility is that from day 5 onwards the system had entered an extended lag phase of L3, however, literature reports suggest that the L3 lag phase typically lasts less than a day [4]. Alternatively, some form of inhibition not yet considered may have prevented L3 growth. A further possibility is that L3 growth did occur but went undetected due to the three-day measurement gap caused by a weekend laboratory closure, although the final biomass concentration is closer to what one would expect after a single L2 growth phase .

In the ‘Dark - CO at 0.7 bar’ run, intended to investigate the D1 state (growth on acetate and CO under dark conditions), the results diverged entirely from expectations. The bacteria utilized available CO (likely with the glucose from the starch extract as *R rubrum* cannot growth chemolithoautotrophically) for growth, leaving acetate untouched. This theory is supported by the small increase of the measured

acetate concentration on day 2, as acetate is a fermentation product of glucose. In other published literature [4], [6], using similar medium composition and reactor setup, however the acetate was utilized during growth.

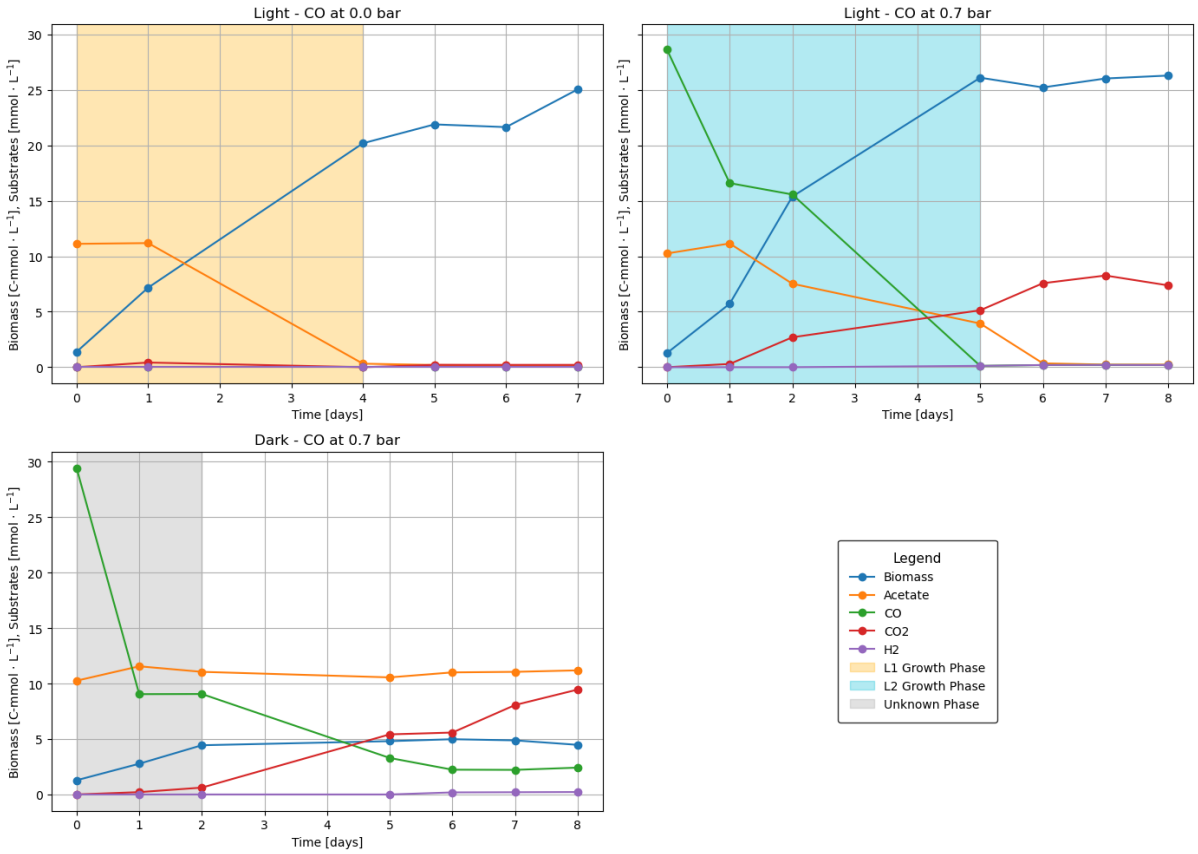

Figure 18: Collected experimental data and the assumed phases of *R. rubrum*

In Figure 19, the predicted biomass and acetate concentrations for the light conditions, both with and without CO, follow the experimental measurements fairly closely. For gases, CO_2 production in the 'Light - CO at 0.0 bar' setup began after one day, however, following the weekend where no measurements were done, it could no longer be detected. This may indicate that *R. rubrum* utilized CO_2 for growth in a metabolic state not considered in the model, that the CO_2 production yields assumed for L2 are higher than in reality (almost certainly the case), or that contamination occurred and another microorganism consumed the CO_2.

In the 'Light - CO at 0.7 bar' setup, a measurement error occurred on day 6, when excess pressure above 1 atm was accidentally released before sampling. This at least partially explains the discrepancy between measured and predicted values of the gas concentrations, although even on days 1 and 2 the measured concentrations were already below model predictions. Hydrogen concentrations in all cases proved difficult to measure, likely due to a combination of factors: limitations of the gas chromatography procedure, as well as effusion losses from the syringe, since an average of three days elapsed between sampling and analysis in the cold cell.

For the 'Dark - CO at 0.7 bar' setup, the model predictions were entirely inaccurate. Contrary to expectations, growth occurred exclusively on CO rather than acetate, and no lag phase was observed.

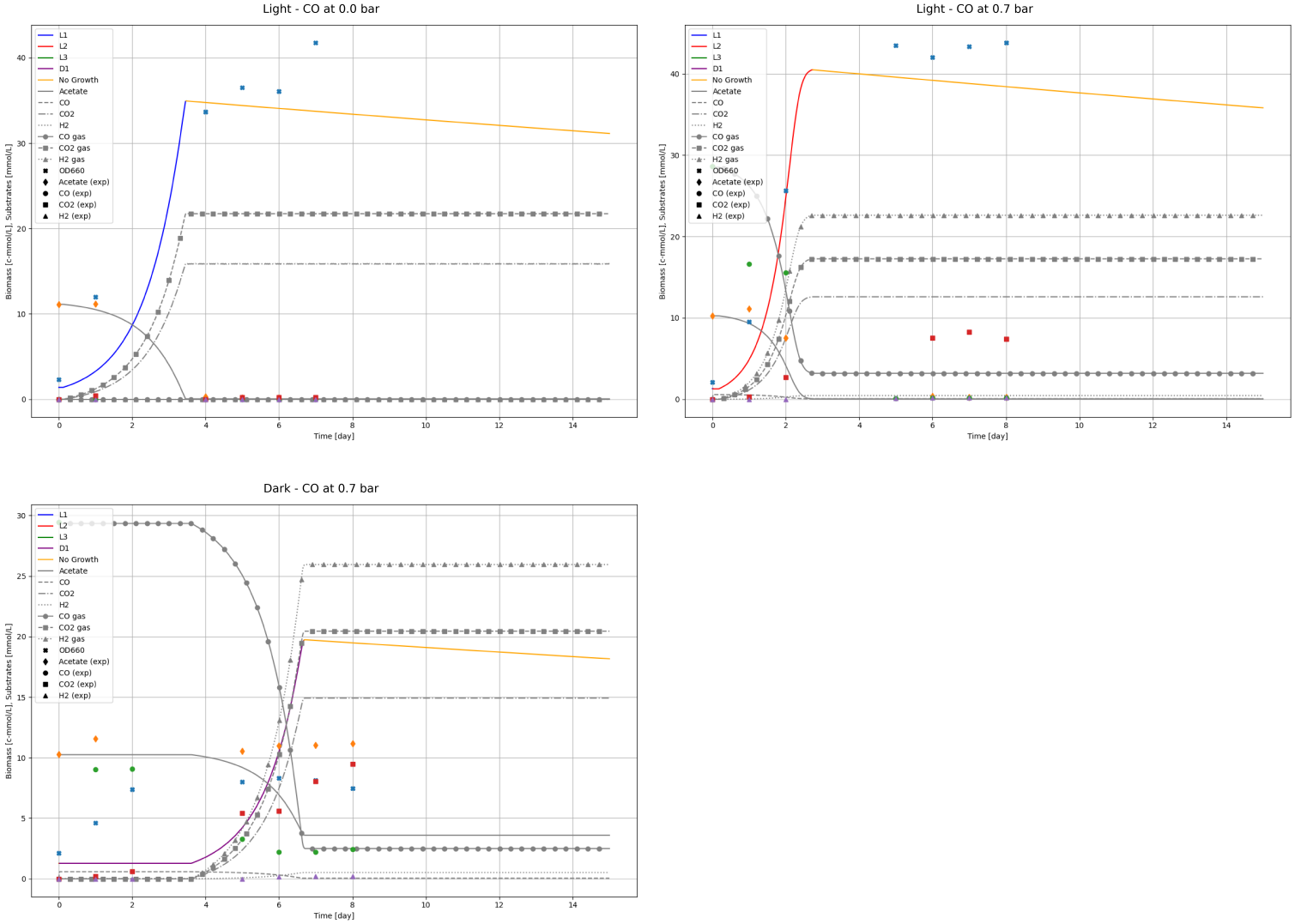

Figure 19: Model compared to the data of the three experiments

5.3. Preliminary Comparison of Possible Optimization Strategies for Maximum Biomass Production

Although the collected data do not fully support the current model, particularly under dark conditions, further investigation is needed to identify additional metabolic states and the conditions that enable them. A short qualitative comparison of *R. rubrum* biomass cultivation can nevertheless be made, with the important caveat that the model requires extension.

For instance, if the observed growth on CO (plus most likely starch extract) under dark conditions is indeed attributable to *R. rubrum*, lets call this a hypothetical D2 state, this would leave acetate, CO_2, and H_2 available at the end of the growth phase, thereby enabling growth from state D0_L1* as shown in Figure 8. Incorporating this extended pathway into the model would not fundamentally alter the bacterium's overall behavior, but it would result in greater acetate availability for subsequent growth phases. Consequently, the L1* phase, normally a relatively short stage dedicated to consuming residual acetate, would become longer and more significant.

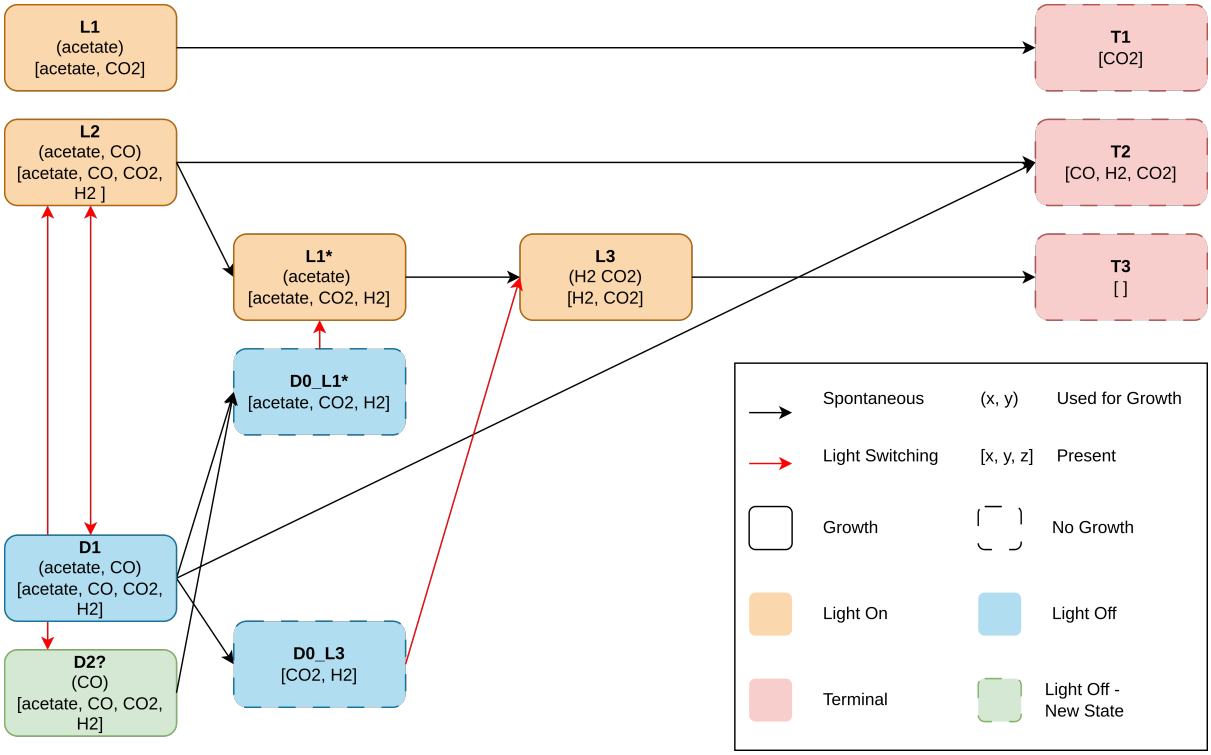

Figure 20: Modified flow chart of the different metabolic states

For the following analysis, results requiring the introduction of new metabolic states are disregarded, and it is assumed instead that environmental conditions restrict growth to the metabolic states already implemented in the model.

To compare different scenarios, several simplifying assumptions were made. The medium volume and acetate concentration were fixed at 0.5 L and 10 mmol/L, respectively. When illumination was applied, it was assumed to be at maximum usable intensity without inhibition (approximately 200 W/m_2). Three different initial CO partial pressures in the headspace were tested: 30%, 60%, and 90%. Evaluation metrics included total reactor runtime, final biomass concentration, the percentage of

runtime under illumination, and the average biomass production rate, defined as the final maximum biomass concentration divided by reactor runtime. Complete substrate utilization was prioritized. Thus, although the biomass production rate is highest during the L2 state (growth on acetate, CO, and light), the reactor was not stopped after this phase but allowed to continue into the L3 state (growth on CO_2 and H_2) until maximum biomass was reached [8].

Three optimization approaches were considered:

- L2-L3: Baseline scenario with continuous illumination. The reactor begins in L2, utilizing acetate and CO, and transitions naturally into L3, consuming the H_2 and CO_2 produced earlier.
- D1-L3: The reactor begins in the dark (D1, growth on acetate and CO). Once maximum biomass is reached, illumination is switched on, allowing growth to continue in L3.
- D1+L3: A two-reactor setup. One reactor operates continuously in the dark, while the other remains illuminated. When the dark reactor (D1) reaches maximum biomass, the biomass is settled, and the remaining medium and gases are transferred to the illuminated reactor, which continues growth in L3. Unlike D1–L3, this approach assumes elimination of lag phases.

The results of these optimizations are shown in Figure 21. As expected, total growth time increased with higher initial CO concentrations. The only exception occurred with 90% CO in the continuously illuminated L2–L3 setup, where residual acetate concentrations at the end of L2 were sufficiently high to inhibit the L3 phase. Final biomass was consistently highest, though only marginally so, in the continuous L2–L3 scenario, apart from the aforementioned exception. This can be explained by the fact that state D1 consumes almost twice as much CO and one and a half times as much acetate per C-mmol of biomass as L2. However, D1 also produces larger amounts of CO_2 and H_2, which prolong L3 growth, resulting in nearly identical total biomass production in the end across scenarios.

The percentage of runtime requiring illumination was lowest in the D1–L3 scenario, but this was primarily due to the extended lag phases in D1. For the same reason, D1–L3 also produced the lowest biomass production rates across all CO concentrations.

In summary, if a two-reactor system is feasible, the D1+L3 setup at high CO concentrations appears optimal, achieving production rates comparable to the continuously illuminated L2–L3 system while reducing illumination time by approximately 20%. If such a setup is not feasible, D1–L3 achieves about half the production rate and requires only half the illumination of L2–L3. However, because L2–L3 produces the same total biomass in a shorter time at comparable cost, it remains the more efficient option in most cases.

[8] If the primary objective is to maximize biomass and/or H_2 and/or CO_2 production as rapidly as possible, and sufficient medium, electricity, and CO are available, then the most effective strategy is simply to operate the reactor in the L2 state and initiate a new batch once this phase is completed. Implementing this approach in a controlled continuously stirred reactor could be particularly interesting. The L2–L3 setup with an initial CO concentration of 90%, in which the L3 state is inhibited by residual CO, illustrates this scenario in Figure 21.

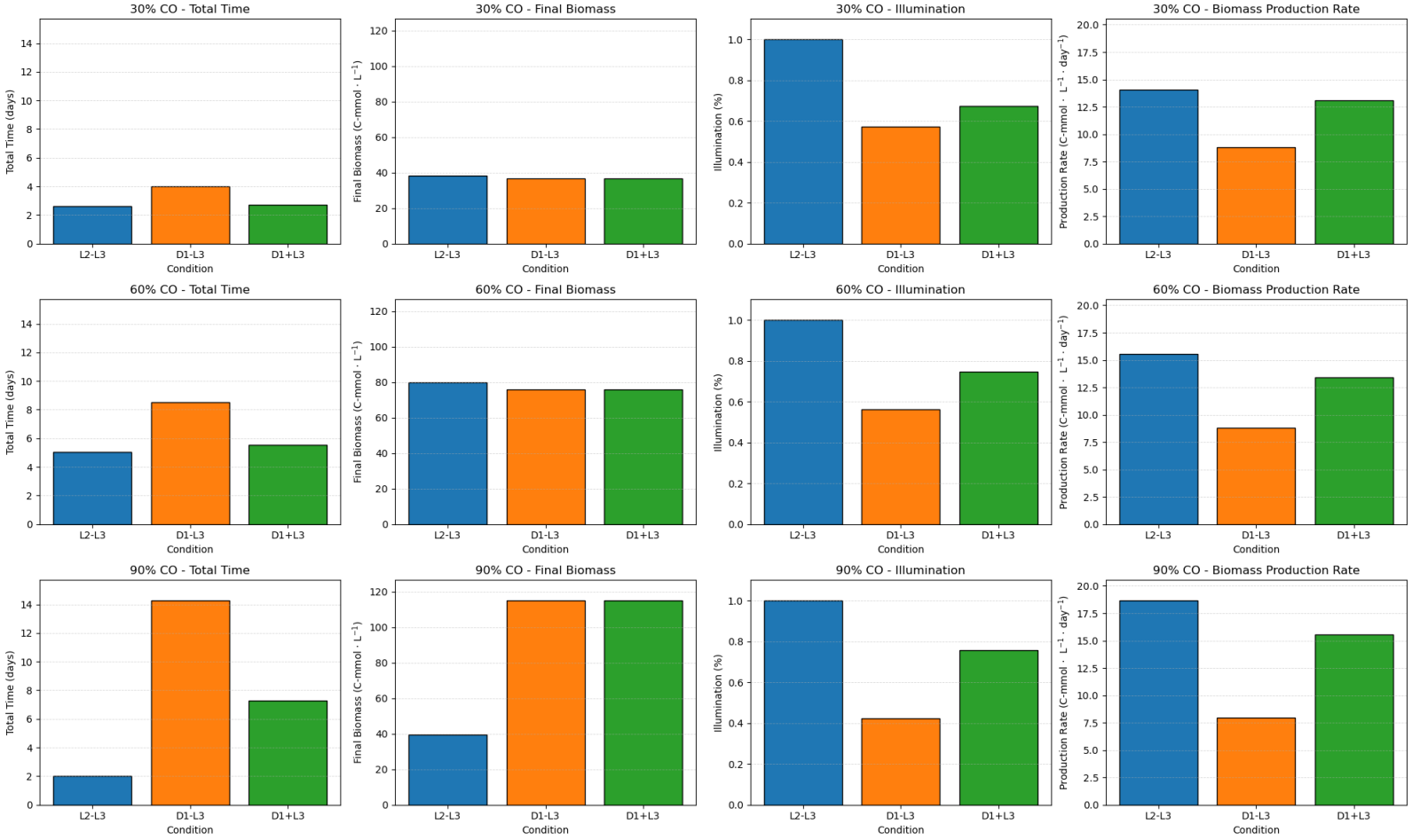

Figure 21: Optimization scenerios

6. Conclusion & Further Research

6.1. Conclusion

The main goal of this thesis was to develop an expandable mathematical model capable of describing the growth of *R rubrum* on different substrates and across various trophic modes. The literature review revealed that most existing research focuses on the organism's potential for hydrogen and bioplastic production, particularly its growth on VFAs and CO under illuminated conditions. For this reason, the model developed in this work was designed to describe the growth of *R. rubrum* under these limited environmental conditions, focusing on the relationship between CO and acetate concentrations, varying light levels, and anaerobic conditions.

After reviewing existing predictive microbiology models, it was determined that, for engineering purposes, an unstructured approach assuming constant bacterial properties would be most appropriate. However, as a possible future extension, the incorporation of variable lag phase durations and growth rates as the cells acclimate to environmental conditions is recommended.

Using published experimental data, the Monod–Ierusalimsky, Haldane, and Aiba models were fitted to describe R. rubrum growth under photolithoheterotrophic conditions in light and chemolithoheterotrophic conditions in darkness, both using acetate as a carbon source and CO as an electron donor. These conditions are referred to as the L2 and D1 states in this document. The fitting resulted in a set of reusable half-saturation and inhibition coefficients, most of which have not been previously published. Available coefficients from the literature primarily concern photoorganoheterotrophic growth with VFAs serving as both carbon source and electron donor [18], [30]. In all cases, the Aiba model provided the best fit and offered a suitable balance between model complexity and usability.

Similarly, published data were used to determine the effect of initial CO concentration on lag phase duration for the same two growth states. The data were fitted with three functions, a first-order, a second-order, and an exponential, with the exponential relationship providing the closest fit. The resulting coefficients could be reused in other modeling efforts as initial estimates, later refined for specific *R. rubrum* strains or experimental setups.

The stoichiometry of the growth reactions for four metabolic states was also determined from the available literature. Many of these values have not been published before. The values presented are approximate and they are likely only meaningful when compared relative to one another and are probably not directly transferable to other systems.

The literature review also showed that several mathematical models for *R. rubrum* already exist, although most focus on a single trophic mode with a single substrate, and when both light and dark phases are considered, the dark phase is often treated as a no-growth period because of its relatively slow rate compared with photosynthesis. A few studies describe the utilization and order of utilization of multiple VFAs as substrates in a single thropic mode or model competition between *R. rubrum* and other aerobic and anaerobic bacteria under different environmental conditions, but they do not differentiate between specific substrates or trophic modes for example within photosynthesis [26], [28]. The model proposed in this thesis could be used to extend such approaches or serve as a bridge between them by integrating detailed, low, process-level data with higher-level engineering models.

Once the derived coefficients were incorporated into the mathematical model, its performance was evaluated against the dataset from which most parameters were obtained. This dataset served as the equivalent of training data. The model accurately predicted the different metabolic states at given times, peak concentrations, and substrate dynamics but also consistently underestimated biomass concentrations. This discrepancy was likely due to biomass values being extrapolated from absorbance measurements, which also affected the calculated yields for the different metabolic states. These yields were probably overestimated. Nevertheless, the test demonstrated that the model can capture the dynamic behavior observed across multiple metabolic modes.

The final version of the model was then validated against an independent dataset collected using a different *R. rubrum* strain and a slightly modified medium that included both dark and light conditions with varying CO concentrations. The model reproduced biomass, acetate, and CO concentrations reasonably well but consistently overestimated CO_2 and H_2 production in the L1 and L2 states. These discrepancies can be partly attributed to measurement methods and frequency, possible experimental setup errors, sample storage conditions, and the three-day sampling gaps over weekends due to laboratory closures. Under dark conditions, however, the observed dynamics diverged completely from model predictions. Growth occurred on CO and likely also on unmeasured fructose present in the yeast extract of the medium, while acetate concentrations remained constant. This may indicate the presence of an unaccounted metabolic state or contamination by another microorganism.

A rough comparison of different reactor configurations was also conducted. The results suggest that, if the goal is to maximize biomass production without limitations on substrate or electricity, the most effective approach is to operate a single illuminated reactor in the L2 state (using acetate and CO), discarding CO_2 and H_2 once the phase concludes. If the goal is to minimize electricity consumption and utilize all available substrates, the best option is a two-reactor system: one maintained in the D1 state (acetate and CO in the dark, producing CO_2 and H_2), followed by settling the biomass and transferring the medium and gases to a second illuminated reactor operating in the L3 state (using CO_2 and H_2). This setup eliminates lag phases, as each reactor's microbial population is already acclimatized to its respective conditions at the start of each batch. If a two-reactor system is not feasible, the second-best option is continuous illumination, starting in L2 and transitioning into L3. This configuration is faster and requires a similar total energy input compared to the D1–L3 approach, where growth begins in the dark and illumination is introduced later.

6.2. Further Research

Further possible research topics can be divided into two categories: investigation of the metabolism and growth of *R. rubrum*, and mathematical approaches to describing its behavior.

Potential questions related to metabolism and growth include:

- As noted before, several parameters remain insufficiently studied, even with the limited environmental conditions used in this report. These include temperature, pH, alternative carbon sources, and the effect of syngas composition, particularly the influence of varying CO_2 and H_2 concentrations. This is especially important for the L3 state, photolithoautotrophy, where

they serves as the electron donor and the carbon source. The role of other, as yet unidentified, compounds that may inhibit *R. rubrum* growth present in real syngas should also be examined.
- The experiment conducted under dark conditions with CO supplementation suggested that, in addition to metabolic states associated with alternative carbon sources, further states may exist. One possible additional state, referred in the document as the D2 state, may for example represent another form of chemolithoheterotrophy utilizing CO and glucose from the yeast extract. Identifying all possible metabolic states, at least using combinations of the available compounds and environmental conditions in the reactor would be important for a reliable model.

The presented mathematical model could be improved in multiple ways:

- Incorporating new experimental data on metabolism and growth directly into the model. This includes implementing inhibition functions for all relevant substrates in every metabolic state, not only for those where data are currently available, and accounting for storage polymer production and consumption.
- Expanding beyond pure culture cultivation. Pure cultures are rarely ideal for industrial applications because they require sterilized media and tightly controlled conditions. While detailed modeling of additional microorganisms may not be necessary in the model, identifying conditions under which *R. rubrum* remains dominant and incorporating this knowledge into the model would make it more realistic.
- Considering the use of structured models that rely more directly on metabolic networks. Such models could provide biologically more accurate predictions than the current unstructured approach.
- Replacing the batch setup with a continuous reactor configuration. Continuous systems are more relevant for industrial applications and would also simplify sampling and data collection, improving both precision and reproducibility.
- Improving numerical methods. The current Python model uses the standard Runge–Kutta–Fehlberg method to solve the system of differential equations. Unfortunately, at low substrate concentrations and high biomass and substrate consumption rates, if the simulation resolution is not sufficiently high, substrate concentrations can become negative within the discretized time step, even when minimum thresholds for growth are enforced. This issue can be mitigated by increasing the resolution, but doing so is computationally expensive and makes later optimization impractical. In last two decade, a new method called automatic differentiation have gained popularity for solving differential equations, offering (near-)exact solutions for complex, stiff problems at a fraction of the computational cost. Re-implementing the current model with such solvers could therefore provide significant benefits.

References

[1] S. Taniguchi and M. D. Kamen, “The oxidase system of heterotrophically-grown rhodospirillum rubrum,” *Biochimica et Buophysica Acta*, 1964.

[2] C. Rudolf and H. Grammel, “Fructose metabolism of the purple non-sulfur bacterium rhodospirillum rubrum: Effect of carbon dioxide on growth, and production of bacteriochlorophyll and organic acids,” *Enzyme and Microbial Technology*, vol. 50, no. 4, pp. 238–246, Apr. 2012, doi: 10.1016/j.enzmictec.2012.01.007.

[3] X. Wang, H. V. Modak, and F. R. Tabita, “Photolithoautotrophic growth and control of CO2 fixation in rhodobacter sphaeroides and rhodospirillum rubrum in the absence of ribulose bisphosphate carboxylase-oxygenase,” *J Bacteriol*, vol. 175, no. 21, pp. 7109–7114, Nov. 1993, doi: 10.1128/jb.175.21.7109-7114.1993.

[4] M. S. Godoy, I. Verdú, S. R. De Miguel, J. D. Jiménez, and M. A. Prieto, “Exploring rhodospirillum rubrum response to high doses of carbon monoxide under light and dark conditions,” *Appl Microbiol Biotechnol*, vol. 108, no. 1, p. 258, Dec. 2024, doi: 10.1007/s00253-024-13079-5.

[5] J. E. Schultz and P. F. Weaver, “Fermentation and anaerobic respiration by *rhodospirillum rubrum* and *rhodopseudomonas capsulata*,” *J Bacteriol*, vol. 149, no. 1, pp. 181–190, Jan. 1982, doi: 10.1128/jb.149.1.181-190.1982.

[6] R. L. Kerby, P. W. Ludden, and G. P. Roberts, “Carbon monoxide-dependent growth of rhodospirillum rubrum,” *J Bacteriol*, vol. 177, no. 8, pp. 2241–2244, Apr. 1995, doi: 10.1128/jb.177.8.2241-2244.1995.

[7] C.-R. Xu, P. Wu, L. Lang, R.-J. Liu, J.-Z. Li, and Y.-B. Ji, “Magnesium ions improving the growth and organics reduction of rhodospirillum rubrum cultivated in sewage through regulating energy metabolism pathways,” *Water Science and Technology*, vol. 72, no. 3, pp. 472–477, Aug. 2015, doi: 10.2166/wst.2015.236.

[8] S. Karmann, S. Panke, and M. Zinn, “Fed-batch cultivations of rhodospirillum rubrum under multiple nutrient-limited growth conditions on syngas as a novel option to produce poly(3-hydroxybutyrate) (PHB),” *Front. Bioeng. Biotechnol.*, vol. 7, p. 59, Apr. 2019, doi: 10.3389/fbioe.2019.00059.

[9] Y. Tian, T. Yue, Y. Yuan, P. K. Soma, and Y. M. Lo, “Improvement of cultivation medium for enhanced production of coenzyme Q10 by photosynthetic rhodospirillum rubrum,” *Biochemical Engineering Journal*, vol. 51, no. 3, pp. 160–166, Sep. 2010, doi: 10.1016/j.bej.2010.06.011.

[10] A. Kramar and M. M. Kostic, “Bacterial secondary metabolites as biopigments for textile dyeing,” *Textiles*, vol. 2, no. 2, pp. 252–264, Apr. 2022, doi: 10.3390/textiles2020013.

[11] T. Shirata Akira, “Isolation of bacteri producing bluish-purple pigment and use for dyeing.” 2000. Available: https://www.jircas.go.jp/sites/default/files/publication/jarq/34-2-131-140_0.pdf

[12] Inc. Metcalf & Eddy, G. Tchobanoglous, and D. Stensel, *Wastewater engineering: Treatment and resource recovery*. 2013.

[13] J. D. Kong, “Modeling microbial dynamics: Effects on environmental and human health,” PhD thesis, University of Alberta, 2017. Available: https://era.library.ualberta.ca/items/0191844e-958e-49fb-bc42-feec802a29ea

[14] M. Muloiwa, S. Nyende-Byakika, and M. Dinka, “Comparison of unstructured kinetic bacterial growth models.” *South African Journal of Chemical Engineering*, vol. 33, pp. 141–150, Jul. 2020, doi: 10.1016/j.sajce.2020.07.006.

[15] N. S. Panikov, “KINETICS, MICROBIAL GROWTH,” *Encyclopedia of Industrial Biotechnology: Bioprocess, Bioseparation, and Cell Technology*, doi: 10.1002/9780470054581.eib378.

[16] O. Revelles, N. Tarazona, J. L. García, and M. A. Prieto, “Carbon roadmap from syngas to polyhydroxyalkanoates in *r**hodospirillum rubrum*,” *Environmental Microbiology*, vol. 18, no. 2, pp. 708–720, Feb. 2016, doi: 10.1111/1462-2920.13087.

[17] N. Ghasem, “Hydrogen evolution from synthesis gas using photosynthetic bacterium, rhodospirillum rubrum, on various acetate concentration,” presented at the Proceedings of the regional symposium on chemical engineering, 2003.

[18] G. Bayon-Vicente, R. Wattiez, and B. Leroy, “Global proteomic analysis reveals high light intensity adaptation strategies and polyhydroxyalkanoate production in rhodospirillum rubrum cultivated with acetate as carbon source,” *Front. Microbiol.*, vol. 11, p. 464, Mar. 2020, doi: 10.3389/fmicb.2020.00464.

[19] P. Ruknongsaeng, A. Reungsang, S. Moonamart, and P. Danvirutai, “INFLUENCE OF NITROGEN, ACETATE AND PROPIONATE ON HYDROGEN PRODUCTION FROM PINEAPPLE WASTE EXTRACT BY rhodospirillum rubrum,” *J. of Wat. & Envir. Tech.*, vol. 3, no. 1, pp. 93–117, 2005, doi: 10.2965/jwet.2005.93.

[20] G. D. Najafpour and H. Younesi, “Bioconversion of synthesis gas to hydrogen using a light-dependent photosynthetic bacterium, rhodospirillum rubrum,” *World J Microbiol Biotechnol*, vol. 23, no. 2, pp. 275–284, Jan. 2007, doi: 10.1007/s11274-006-9225-2.

[21] K. T. Klasson, J. P. Cowger, C. W. Ko, J. L. Vega, E. C. Clausen, and J. L. Gaddy, “Methane production from synthesis gas using a mixed culture ofR. Rubrum m. Barkeri, and m. formicicum,” *Appl Biochem Biotechnol*, vol. 24–25, no. 1, pp. 317–328, Mar. 1990, doi: 10.1007/BF02920256.

[22] Y. S. Do *et al.*, “Growth of *rhodospirillum rubrum* on synthesis gas: Conversion of CO to h_2 and poly-β-hydroxyalkanoate,” *Biotech & Bioengineering*, vol. 97, no. 2, pp. 279–286, Jun. 2007, doi: 10.1002/bit.21226.

[23] R. L. Uffen, “Effect of low-intensity light on growth response and bacteriochlorophyll concentration in *rhodospirillum rubrum* mutant c,” *J Bacteriol*, vol. 116, no. 2, pp. 1086–1088, Nov. 1973, doi: 10.1128/jb.116.2.1086-1088.1973.

[24] M. Cerruti, J.-H. Kim, M. Pabst, M. C. M. Van Loosdrecht, and D. G. Weissbrodt, “Light intensity defines growth and photopigment content of a mixed culture of purple phototrophic bacteria,” *Front. Microbiol.*, vol. 13, Oct. 2022, doi: 10.3389/fmicb.2022.1014695.

[25] B. S. Ross and R. W. M. Pott, “Investigating and modeling the effect of light intensity on *rhodopseudomonas palustris* growth,” *Biotech & Bioengineering*, vol. 119, no. 3, pp. 907–921, Mar. 2022, doi: 10.1002/bit.28026.

[26] P. C. Segura, R. Wattiez, A. Vande Wouwer, B. Leroy, and L. Dewasme, “Dynamic modeling of rhodospirillum rubrum PHA production triggered by redox stress during VFA photoheterotrophic assimilations,” *Journal of Biotechnology*, vol. 360, pp. 45–54, Dec. 2022, doi: 10.1016/j.jbiotec.2022.10.014.

[27] J.-F. Cornet, L. Favier, and C.-G. Dussap, “Modeling stability of photoheterotrophic continuous cultures in photobioreactors,” *Biotechnol Progress*, vol. 19, no. 4, pp. 1216–1227, Sep. 2008, doi: 10.1021/bp034041l.

[28] A. Alloul *et al.*, “A novel mechanistic modelling approach for microbial selection dynamics: Towards improved design and control of raceway reactors for purple bacteria,” *Bioresource Technology*, vol. 390, p. 129844, Dec. 2023, doi: 10.1016/j.biortech.2023.129844.

[29] M. Ahnert, T. Schalk, H. Brückner, J. Effenberger, V. Kuehn, and P. Krebs, “Organic matter parameters in WWTP – a critical review and recommendations for application in activated sludge modelling,” *Water Science and Technology*, vol. 84, no. 9, pp. 2093–2112, Nov. 2021, doi: 10.2166/wst.2021.419.

[30] M. Cerruti, “Harnessing the metabolic versatility of purple non-sulfur bacteria,” *Dissertation (TU Delft)*, 2022, doi: 10.4233/uuid:c98876c1-aa83-4c8d-9816-191daf5cc423.

[31] R. Sander, “Compilation of henry’s law constants (version 5.0.0) for water as solvent,” *Atmos. Chem. Phys.*, vol. 23, no. 19, pp. 10901–12440, Oct. 2023, doi: 10.5194/acp-23-10901-2023.

[32] V. Veljković and M. Lazic, “Oxygen transfer in flasks shaken on orbital shakers,” *Hemijska industrija*, vol. 49, pp. 265–272, Jan. 1995.

[33] U. Maier and J. Büchs, “Characterisation of the gas–liquid mass transfer in shaking bioreactors,” *Biochemical Engineering Journal*, vol. 7, no. 2, pp. 99–106, Mar. 2001, doi: 10.1016/s1369-703x(00)00107-8.

[34] M. Chaudhry, “Lessons in bioreactor scale-up, part 5: Theoretical and empirical correlations for predicting the mass-transfer coefficient in stirred-tank bioreactors,” *BioProcess International*, 2025, Available: https://www.bioprocessintl.com/bioreactors/lessons-in-bioreactor-scale-up-part-5-theoretical-and-empirical-correlations-for-predicting-the-mass-transfer-coefficient-in-stirred-tank-bioreactors

A. Further Model Details

A.1. Other Possible Parameters

Here, some parameters with data extracted from existing literature are presented, but were ultimately not included in the model due to the high degree of uncertainty.

A.1.1. Effect of Magnesium

The study by Xu et al. [7] investigated the effect of different magnesium concentrations on the growth of *R. rubrum* [9]. Growth was observed even without magnesium supplementation, which is reasonable given that the wastewater from the soybean factory likely already contained some magnesium.

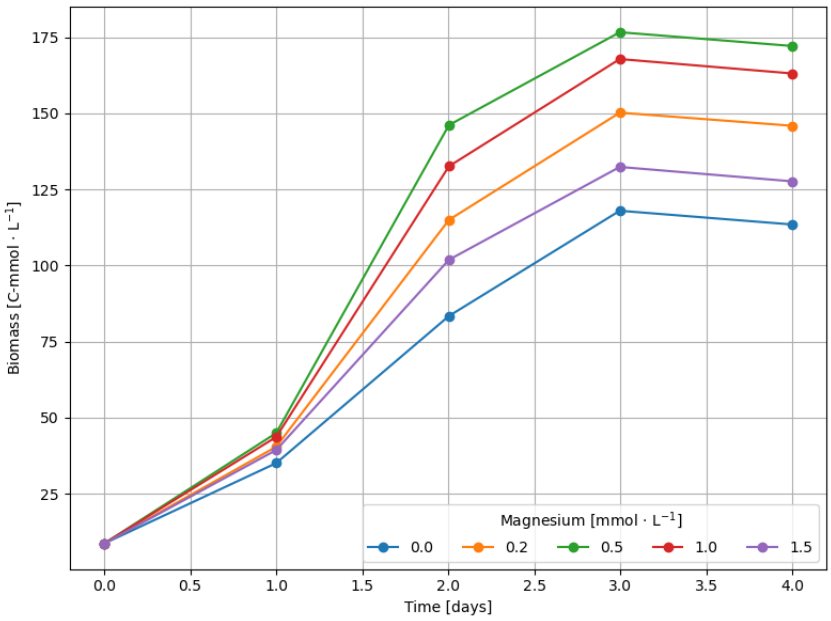

Figure 22: Effect of different magnesium concentrations

Since the growth rate was not zero at zero concentration, an offset was required in the mathematical model. This offset, μ_0, was assigned the value of the growth rate measured at zero concentration and was incorporated into the three mathematical models compared, shown in Equation 29 - Equation 31.

$$\mu = \mu_{max} \left[\left(\frac{S}{S + K_s} \right) \left(\frac{K_i}{S + K_i} \right) + \frac{\mu_0}{\mu_{max}} \right] \tag{29}$$

[9] The paper does not specify which form of magnesium sulfate was used, therefore, it was assumed to be magnesium sulfate heptahydrate, its most common form. This assumption is relevant for the conversion from g/L to mmol/L. However, even if a different form had been used, the quality of the model fits, as measured by R^2, would remain unaffected, although the exact model parameters would differ.

$$\mu = \mu_{max} \left[\frac{S}{S + K_s + \frac{S^2}{K_i}} + \frac{\mu_0}{\mu_{max}} \right] \tag{30}$$

$$\mu = \mu_{max} \left[\left(\frac{S}{S + K_s} \right) e^{-\frac{S}{K_i}} + \frac{\mu_0}{\mu_{max}} \right] \tag{31}$$

The results of the model fitting for the different magnesium concentration levels are shown inFigure 23.

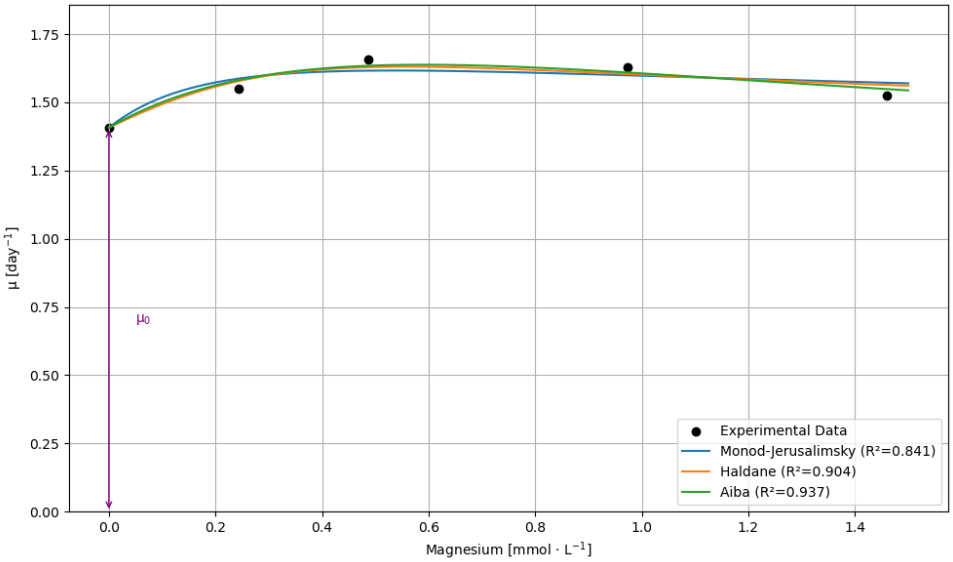

Figure 23: Relationship between supplemented magnesium concentration and specific growth rate

The parameters of the fitted models are presented in Table 15

Table 15: Results of parameter fitting for different supplemented magnesium concentrations.Results of the parameter fitting of different magnesium concentrations supplemented

Model	mu_max	K_s	K_i	R2
Monod-Jerusalimsky	0.837446	0.536410	0.536368	0.840663
Haldane	1.5	1.591317	0.194883	0.903577
Aiba	1.5	1.330574	0.851767	0.936823

A.1.2. Effect of Syngas

Here, the half-saturation and inhibition coefficients for a specific syngas composition are calculated based on the data extracted from the study by Karmann et al. [8].

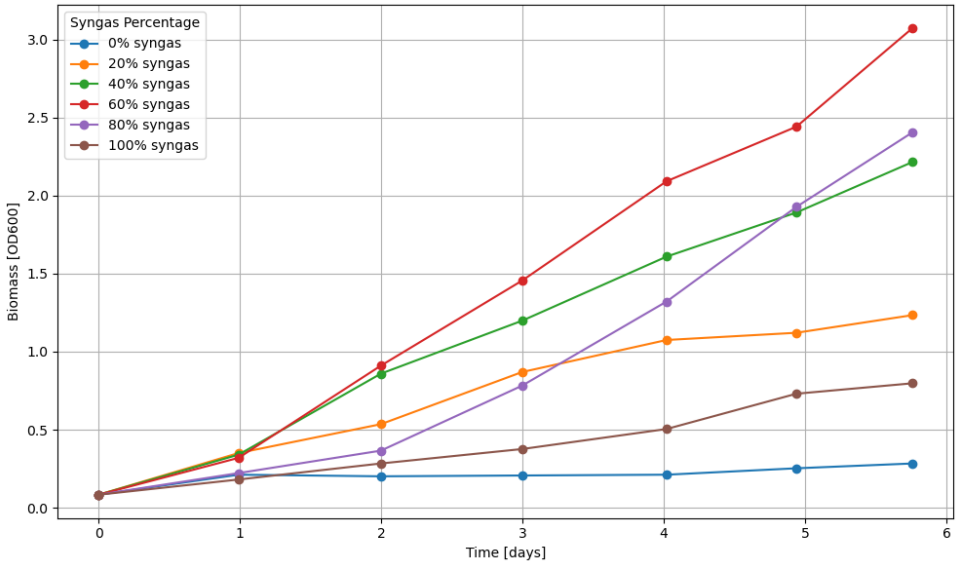

Figure 24: Effect of different syngas concentrations

The gas ratios after dilution are presented in Table 16.

Table 16: Different gas ratios after dilution

Syngas [%]	CO [bar]	H_2 [bar]	CO_2 [bar]	N_2 [bar]
20	0.08	0.08	0.02	0.02
40	0.16	0.16	0.04	0.04
60	0.24	0.24	0.06	0.06
80	0.32	0.32	0.08	0.08
100	0.40	0.40	0.10	0.10

The fitted model and the corresponding parameters are presented in Figure 25 and Table 17.

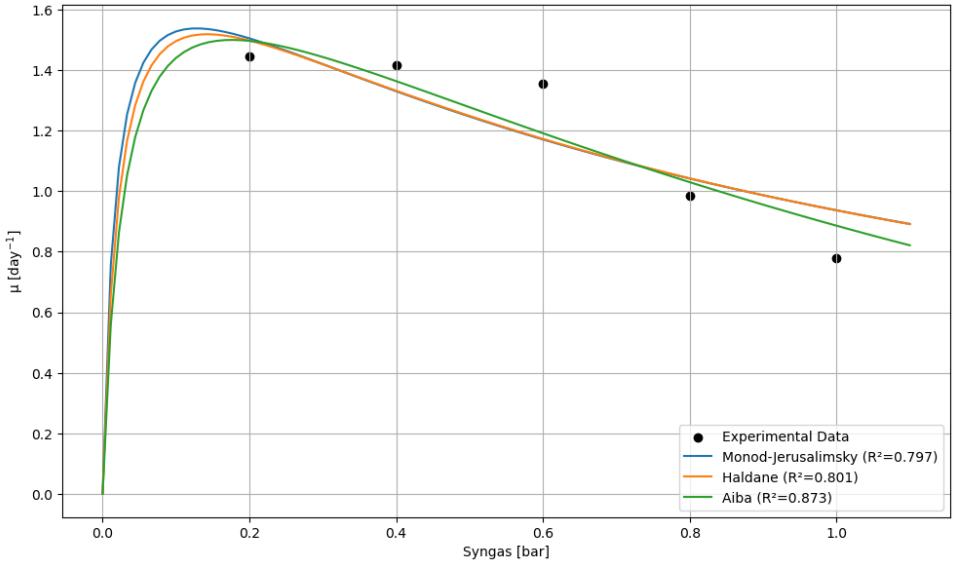

Figure 25: Effect of differerent syngas concentartions on the maximum growth rate of *R. rubrum*

Table 17: Results of the model parameter fitting for syngas

Model	mu_max	K_s	K_i	R2
Monod-Jerusalimsky	2	0.017947	0.911860	0.796529
Haldane	2	0.022548	0.898873	0.801450
Aiba	2	0.028341	1.272144	0.873381

A.2. Henry's Coefficents of the Different Gases at 30°C

The temperature dependence of the dimensionless Henry's law coefficient H_{cc} is given by:

$$H_s(T) = H_s^\circ \cdot \exp\left(-\frac{\Delta_{\text{sol}}H}{R}\left(\frac{1}{T} - \frac{1}{T^\circ}\right)\right) \tag{32}$$

Where:

- $H_s(T)$: Henry's constant at temperature T in K
- H_s°: value at reference temperature $T^\circ = 298.15\,K$
- $\Delta_{\text{sol}}H$: enthalpy of dissolution (J/mol)
- $R = 8.314\,\text{J/mol·K}$
- $T = 303.15\,K$ (30 °C)

Using the Henry's coffecients from [31] at standard conditions to calculate their value at 30°C:

Table 18: Input values for Henry's

Gas	H_{cc} [25 °C]	$\Delta_{sol}H$ [kJ/mol]	H_{cc} [30 °C]
CO	0.023	-12	0.0212
CO_2	0.83	-19	0.731
H_2	0.019	-1.2	0.01885

A.3. kLa

Given the relativly slow growth rate of R. rubrum compared to gas disolution, finding a precise volumetric mass transfer coefficient is not that important. If the volumetric mass transfer of oxygen as well as the different diffusivity of the different gases, rough approximation for the kLa value for the different non-oxygen gases [32], [33], [34] as shown in Equation 33

$$k_L a(i) \approx k_L a(\mathrm{O_2}) \sqrt{\frac{D_i}{D_{\mathrm{O_2}}}} \tag{33}$$

The stirrer was running with an estimated 40 rpm for which the $k_L a(\mathrm{O_2})$ is approximately 144 day^{-1}, and the diffusivity if at standard condtion, $\mathrm{H_2} = 4.50,\ \mathrm{CO} = 2.03,\ \mathrm{CO_2} = 1.92,\ \mathrm{O_2} = 2.10$.

Table 19: Volumetric mass transfer of the different gases

Gas	kLa [day^{-1}]
H_2	211
CO	142
CO_2	137

Ultimately, it was found that gas transfer is not a limiting factor for growth, and setting gas transfer ratios to effectively infinity did not alter the model predictions.

B. Code

Model version	1.0
Python version	3.12.9
Matplotlib version	3.10.1
Numpy version	2.2.4
Scipy version	1.15.2
Link to code and collected data	https://tud365-my.sharepoint.com/:f:/g/personal/kkiss_tudelft_nl/ElKTSYKXMtZFtR1seWl-65UBRCjIh0y23jqpCg18p3kJ4Q?e=kiRauS